$$\lambda(m) = D_v\left[\left(\frac{(q+q_R)^2}{4} + 2\beta\frac{qq_R}{1-\beta}\right)^{1/2} + \frac{q_R - q}{2}\right]^2 - D_v q^2 - \tau_v^{-1}, \tag{4.23}$$

where $\beta = c_t^2/c_l^2$, $q_R = R_v/D_v\gamma$.

To calculate the critical value of the pump parameter we expand Eq. (4.22) into a power series with respect to $\lambda / qc_{l,t}$, $(\lambda + \tau_v^{-1}) / D_v q^2 \ll 1$. Then, we obtain the following soft mode ($m \gg 1$):

$$\lambda = -\frac{8D_v m}{r_{eff}^2} - \tau_v^{-1} + \frac{4R_v\sqrt{m}}{\gamma r_{eff}(1-\beta)}. \tag{4.24}$$

It is seen from Eq. (4.24) that GDI develops only when $R > 0$, i. e., as follows from Eq. (4.21), when $\theta_0 < 0$. The growth rate reaches the maximum value

$$\lambda_{max} = R_v^2/(2\gamma^2 D_v(1-\beta)^2) - \tau_v^{-1},$$

at

$$m = m_0 = (R_v r_{eff}/4\gamma D_v(1-\beta))^2. \tag{4.25}$$

For the critical value of the pump parameter $R_{cr}(m)$, determined from the condition $\lambda = 0$ we obtain the following expression

$$R_{cr}(m) = (8D_v m/r_{eff}^2 + \tau_d^{-1})\gamma r_{eff}(1-\beta)/4\sqrt{m}. \tag{4.26}$$

Thus at $R > R_{cr}(m)$ the coupled fields of deformation (Eq. (4.18)) and vacancy concentration (Eq. (4.19)) start to grow exponentially in time, forming the surface radial ring "star"-structure.

It follows from Eq. (4.26) that the initial ray structure appearing after reaching the minimum critical value of the pump parameter contains m_{init} rays

$$m_{init} = r_{eff}^2\tau_d^{-1}/8D_v = \left(\frac{R_{min}}{R_v}\right)^2 m_0, \tag{4.27}$$

where R_{min} is determined by the expression

$$R_{min} = (1-\beta)\gamma(D_v\tau_d^{-1}/2)^{1/2}. \tag{4.28}$$

If $R_v > R_{min}$, then several structures with different number of rays m are excited simultaneously, and the overall picture of the deformation can be obtained by summing over m:

$$\xi \sim \sum_m \left(\frac{r}{r_{eff}}\right)^m \exp\left(-\frac{r^2}{r_{eff}^2} + \lambda(m)t\right)\cos m\varphi = \sum_m \xi_m \cos m\varphi. \tag{4.29}$$

At a given value of r / r_{eff} the term ξ_m, for which $\partial\xi_m / \partial m = 0$ provides maximum contribution to the sum (4.29). From this condition we obtain the value of m_{max}, or the number of rays in the harmonic, having the largest amplitude at a given value of r / r_{eff}. Using Eq. (4.24) for $\lambda(m)$, for m_{max} at the end of the pulse we obtain the following expression

$$m_{max} = m_0\left(1 - r_{eff}^2 \ln\left(\frac{r_{eff}}{r}\right)/8D_v\tau_p\right)^{-2}, \tag{4.30}$$

for $r \to 0$, $m_{max} \to 0$ and for $r \to r_{eff}$, $m_{max} \to m_0$.

Thus, with the increase of the distance from the center of the spot the harmonics containing larger and larger number of rays dominate.

Apart from the ray-star solution, the system of Eqs. (4.13) and (4.15) with the boundary conditions (4.6a), (4.16), (4.17) has the radial-ring solutions which are obtained by substituting $(r / r_{eff})^m \cos m\varphi \to J_m(qr)\cos m\varphi$ in Eqs. (4.18) and (4.19), where $J_m(qr)$ is the first type Bessel function of the mth order, $q \gg r_{eff}^{-1}$ is the wave number. At $m = 0$ this solution corresponds to the concentric ring structure. If there is some preferred direction on the surface then one should replace $(r / r_{eff})^m \cos m\varphi \to e^{iqx}$ in the solution of Eqs. (4.18 - 4.20), which corresponds to a grating structure. For these solutions the dependence of λ on wave number q is determined by Eq. (4.22), similar to the case of radial rays (see Fig. 2a for the visual representation of possible structures formed in vacancy GDI under different conditions).

4.1.3. Comparison of Theoretical and Experimental Results

We interpret the experimentally observed structures of Sec. 4.1.1 as the DD structures, formed due to the vacancy GDI. The axial symmetry of the laser field, together with the isotropic (polycrystal) structure of the metal surface leads to formation of the axially symmetric vacancy-deformational structure, i.e., ray-star structure. (Consideration of influence of the crystallographic symmetry on the vacancy GDDI will be given in Sec. 4.3). As it follows from the above analysis, the surface relief must be modulated, which in fact does take place. The vacancy pileups arising due to the GDI in the valleys of the surface relief must lead eventually to void formation (Secs. 5.1 and 5.2). Periodic void formation is indeed observed in these experiments (see Fig. 11e).

Let us make numeric estimates of the number of rays m_{max}, critical vacancy concentration n_{cr} and the time of GDI development. From Eq. (4.28) for R_{min} (for the case of nonstationary temperature distribution) at $\beta = 0.5$, $t = \tau_p$, $\gamma = 10^4$ cm^{-1}, $E_0 / kT_0 \approx 10^2$, $D_v \approx 10^{-5}$ cm^2·s^{-1}, $\tau_p \approx 10^{-2} - 10^{-3}$ s we obtain $R_{min} \approx 10^3$ s^{-1}. Assuming that $n_{cr} = g_0\tau_v$ ($\tau_p \gg \tau_v$) or $n_{cr} = g_0\tau_p$ ($\tau_v \gg \tau_p$), where g_0 is defined by Eq. (4.21) with $R = R_{min}$, at $|\theta_0| = |\theta_v| =$

10^{-10} erg, $c_l^2 = 10^{11}$ cm^2·s^{-2}, $\rho \sim 5$ g·cm^{-3} we obtain the following estimate for n_{cr}:

$$n_{cr} \approx 5 \times 10^{18} \text{ cm}^{-3}.$$

At $r_0 \approx 10^{-1}$ cm, $r_{eff} \approx 10^{-2}$ cm, we have $m_{init} \approx 10^2$. From Eq. (4.27) at $R_v = 3R_{min}$ we have $m_0 \approx 10^3$, which corresponds, by the order of magnitude, to the experimentally measured number of rays. The time of GDI development is $\lambda_{max}^{-1} \cong \tau_v / 10 \approx 10^{-3}$ - 10^{-4} s.

We carried out computer calculations of the resultant deformation field on the surface existing by the end of the laser pulse for different values of r / r_{eff}, using Eq. (4.29) in relative units

$$\xi = \sum_{m=m_1}^{m_2} \cos m\varphi \exp\left[2\frac{R_v}{R_{min}}\frac{\tau_p}{\tau_v}\left(\frac{m}{m_{init}}\right)^{1/2} - m\ln\frac{r_{eff}}{r} - \frac{\tau_p}{\tau_v}\frac{m}{m_{init}}\right].$$

The summation is performed over the number of harmonics m from m_1 to m_2, for which $\lambda(m) > 0$ ($m_{1,2} = [R_v / R_{min} \mp ((R_v / R_{min})^2 - 1)^{1/2}]^2 m_{init}$) at light intensity exceeding the threshold $R_v = 1.1R_{min}$. Then, at $\tau_p \tau_v^{-1} \approx 30$, $m_{init} = 50$, $m_1 = 20$, $m_2 = 200$. At $r_{eff} / r > 1$ the summation can be extended up to $m_0 = 60$. The results of the computations are shown in Fig. 12. It is seen that with the increase of the distance from the center, multiplication of the number of rays via bifurcations of them takes place. This behavior corresponds to the experimental findings (Fig. 11c).

Thus, the qualitative and quantitative correspondence of the theoretical and experimental results enables one to make the conclusion that the formation of the periodic ray structures on the surface of a metal under the action of millisecond laser pulses occurs due to the development of vacancy GDI.

It is seen from Eqs. (4.21) and (4.24) that GDI occurs only under the condition $R_v > 0$, i.e., $\theta_0 < 0$. In the case of thermal-fluctuation generation rate in Eq. (4.3) $E_0 = E_v$ and $\theta_0 = \theta_v < 0$, so that this condition is automatically fulfilled.

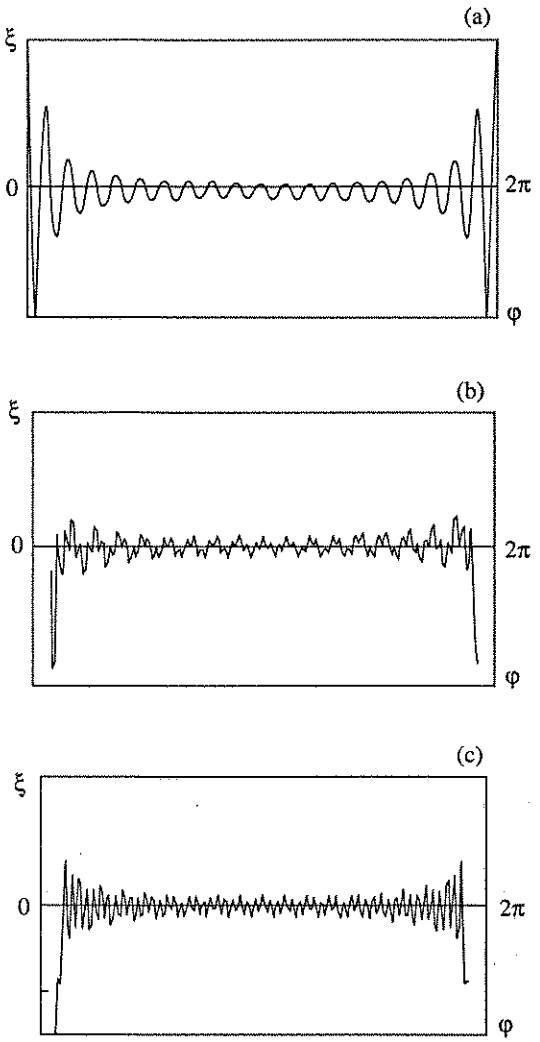

Fig. 12. *Dependence of the amplitude of surface deformation "star"-structure due to vacancy GDI on the angle φ at different values of r (numerical calculation according to Eq. (4.29a): the number of rays m = 20, $r_{eff}/r = 1.5$ (a); ray multiplication via bifurcation, $r_{eff}/r = 1.13$ (b); the number of rays m = 56, $r_{eff}/r = 1.1$ (compare with Fig. 4b) (c).*

4.2. Vacancy Diffusion-Deformational Instability (DDI) in Films

In thin plates and films the bending deformation may be significant for development of GDI and DDI. This circumstance is demonstrated here for DDI in the case of unsupported plate (film) [75] and in Sec. 4.3 for DDI in the case of a thin film on substrate. The case of GDI due to bending deformation of the film was considered by us in earlier works [28, 29].

Let us consider a thin metal plate of thickness h. The z-axis is directed perpendicular to the plate, and the plane $z = 0$ coincides with the middle plane of the plate. The laser radiation acts upon the surface $z = h / 2$, creating vacancies. The mechanism of generation of vacancies is insignificant, and we assume the generation rate G_v in the right-hand side of Eq. (4.6) for n_v spatially uniform along the surface.

In this case the boundary conditions are given by

$$\left(\frac{\partial n_v}{\partial z}\right)_{z=\frac{h}{2}} = \left(\frac{\partial n_v}{\partial z}\right)_{z=-\frac{h}{2}} = 0. \qquad (4.31)$$

The bending deformation of the film is described by the bending coordinate ζ, or displacement of the points of the middle plane along the z-axis. Under the bending deformation the strain is coupled with the bending coordinate by the relation

$$\text{div } \mathbf{U} = -z\nu\Delta\zeta, \qquad (4.32)$$

where $\nu = (1 - 2\sigma) / (1 - \sigma)$, σ is the Poisson coefficient.

The nonlinear equation for the bending coordinate follows from Ref. [76], if one takes into account the force acting on the film due to vacancy-elastic continuum interaction energy (cf. Eq. (1.1)):

$$\frac{\partial^2\zeta}{\partial t^2}+\frac{c^2h^2}{12}\Delta_\parallel^2\zeta-\frac{1}{\rho}\left(\sigma_{xx}\frac{\partial^2\zeta}{\partial x^2}+\sigma_{yy}\frac{\partial^2\zeta}{\partial y^2}+2\sigma_{xy}\frac{\partial^2\zeta}{\partial x\partial y}\right)\Bigg|_{z=0}$$
$$=-\frac{\theta_v}{\rho h}\int_{-h/2}^{h/2}\frac{\partial n_v}{\partial z}dz. \tag{4.33}$$

Here $c^2 = E / \rho(1 - \sigma^2)$, E is Young's modulus, $\Delta_\parallel = \frac{\partial^2}{\partial x^2}+\frac{\partial^2}{\partial y^2}$ is the two-dimensional Laplace operator.

The stress tensor

$$\sigma_{jk}=-\frac{E}{1-\sigma^2}\left[\left((1-\sigma)\frac{\partial^2\zeta}{\partial x_j\partial x_k}+\sigma\delta_{jk}\Delta_\parallel\zeta\right)z\right.$$
$$\left.+(1+\sigma)\alpha T\delta_{jk}+N_{jk}\right].$$

Here

$$N_{xx}=-\frac{1}{2}\left(\frac{\partial\zeta}{\partial x}\right)^2-\frac{1}{2}\sigma\left(\frac{\partial\zeta}{\partial y}\right)^2,$$
$$N_{yy}=-\frac{1}{2}\left(\frac{\partial\zeta}{\partial y}\right)^2-\frac{1}{2}\sigma\left(\frac{\partial\zeta}{\partial x}\right)^2, \tag{4.34}$$
$$N_{xy}=(1-\sigma)\left(\frac{\partial\zeta}{\partial x}\frac{\partial\zeta}{\partial y}\right).$$

Eqs. (4.6) and (4.31) form a closed system of equations describing the bending deformations interacting with the vacancy field.

Note that it follows from Eq. (1.1) that the tangential components of the forces exist $\mathbf{F}_{x,y} \sim (\text{grad } n)_{x,y}$, which yield additional contributions to the r.h.s. of Eq. (4.33) which are by a factor of $\gamma^2 d^2 \gg 1$ smaller than the terms taken into account (here γ is the decay constant of n_v along z, d is the period (along the surface) of vacancy structure, developed due to the instability considered).

We consider first the linear regime. Let us represent the variables in the form

$$n_v = n_0 + n_1,\ \zeta = \zeta_0 + \zeta_1,\ \mathbf{U} = \mathbf{U}_0 + \mathbf{U}_1,$$

where n_0, ζ_0, and $\mathbf{U}_0$ are spatially uniform along the surface solutions and n_1, ζ_1, and $\mathbf{U}_1$ are small spatially nonuniform perturbations.

Consider first the spatially uniform distribution of vacancies. From Eq. (4.6) we obtain the equation for n_0

$$D_v\frac{\partial^2 n_0}{\partial z^2}-\frac{n_0}{\tau_v}+G_v=0. \tag{4.35}$$

Under the action of laser radiation on the surface $z = h / 2$ with effective thermal runaway from the surface $z = -h / 2$ at times $t > h^2 / \chi$ the temperature is a linear function of z:

$$T = T_0 - \Delta T\left(\frac{h}{2}-z\right)/h.$$

Under the condition $\gamma\sqrt{D_v\tau_v} \ll 1$ the solution of Eq. (4.35) with the boundary conditions (4.31) can be represented in a simplified form

$$n_0(z) \simeq g\tau_v\exp\left[-\gamma\left(\frac{h}{2}-z\right)\right]$$
$$\equiv n_0\exp\left[-\gamma\left(\frac{h}{2}-z\right)\right], \tag{4.36}$$

where $\gamma = E_0\Delta T / kT_0^2 h$.

In the equation for n_1 we take into account that under the conditions of the experiments of interest ($\alpha T \sim 10^{-3}$) the linear term in the brackets in Eq. (4.33) proportional to σ_{jk} is a factor of $10^4(h / d) \gg 1$ less than the second term in the l.h.s. of Eq. (4.33), here $d \sim h$ (see Eq. (4.49)).

We restrict ourselves to the case for which the coefficient of surface diffusion $D_\parallel \gg D_v$, where D_v is the coefficient of the bulk diffusion (this assumption is not principal and is made only for the sake of simplicity of treatment).

We introduce the notation

$$n_1 \equiv n_1\left(z=\frac{h}{2}\right),\ n_1\left(-\frac{h}{2}\right) \ll n_1\left(\frac{h}{2}\right).$$

Then, the linearized system of equations for n_1, ζ_1 has the form

$$\partial^2\zeta/\partial t^2+\frac{c^2h^2}{12}\Delta_\parallel^2\zeta_1=-\frac{\theta_v n_1}{\rho h},$$
$$\frac{\partial n_1}{\partial t}=D_\parallel\Delta_\parallel n_1-\tau_v^{-1}n_1-n_0\theta_v h\nu D_\parallel\Delta_\parallel^2\zeta_1/2kT. \tag{4.37}$$

The spatial symmetry of the problem determines the form of the solution n_1 and ζ_1. The simplest case corresponds to the one-dimensional geometry, with the x-axis being the preferred direction. We consider this case first in the linear regime.

The solution of Eq. (4.37) is developed in the form

$$\zeta_1(q) = A_q\exp(iqx+\lambda t)+\text{c. c.},$$
$$n_1(q) = B_q\exp(iqx+\lambda t)+\text{c. c.}, \tag{4.38}$$

where A_q, B_q = const. Substituting Eq. (4.38) in Eq. (4.37), under the condition $\lambda^2 \ll q^4c^2h^2 / 12$ we obtain the dispersion equation for λ

$$\lambda = R_v - D_\parallel q^2 - \tau_v^{-1}, \tag{4.39}$$

where the external pump parameter is given by

$$R_v = 6\theta_v^2\nu n_0 D_\parallel/\rho c^2 kT_0 h^2. \tag{4.40}$$

Thus, to each wave number q corresponds the critical value of the pump parameter $R_{cr} = R_{cr}(q)$, such that at

$R_v > R_{cr}(q)$ one has $\lambda(q) > 0$, i.e., exponential growth of the Fourier amplitudes of the coupled fields of bending deformation and vacancy concentration is realized. The threshold of the instability is determined by the condition

$$R_v > \tau_v^{-1},$$

i.e., concentration of vacancies n_0 exceeds the critical value n_{cr}:

$$n_{cr} = \rho c^2 k T_0 h^2 / 6\theta_v^2 \nu D_\parallel \tau_v. \quad (4.41)$$

A stabilization of vacancy DDI occurs due to the nonlinearity of the bending deformations. In the one-dimensional case, one has (in the stationary case) the following equation

$$\frac{c^2 h^2}{12}\frac{\partial^4 \zeta_1}{\partial x^4} - \frac{c^2}{2}\frac{\partial^2 \zeta_1}{\partial x^2}\left(\frac{\partial \zeta_1}{\partial x}\right)^2 = -\frac{\theta_v n_1}{\rho h}. \quad (4.42)$$

The equation for n_1 follows from Eq. (4.37) at $\partial n_1 / \partial t = 0$. Substituting (4.38), where $\lambda = 0$ into Eq. (4.42) and into stationary equation (4.37), in the uncoupled harmonics approximation we obtain the expression for the stationary Fourier amplitude of the bending deformation field

$$A_q = \frac{h}{\sqrt{6}}\left(\frac{R_v}{D_\parallel q^2 + \tau_v^{-1}} - 1\right)^{1/2} \quad (4.43)$$

and also the expression for the Fourier amplitude of the vacancy concentration field

$$B_q = -A_q \frac{R_v \rho c^2 h^3 q^4}{12|\theta_v|(D_\parallel q^2 + \tau_v^{-1})}. \quad (4.44)$$

It is seen from Eq. (4.39) that at $n_0 > n_{cr}$ the maximum value of the wave number exists

$$q \equiv q_0 = \left(\frac{R_v - \tau_v^{-1}}{D_\parallel}\right)^{1/2}, \quad (4.45)$$

such that the amplitudes of Fourier harmonics with $q > q_0$ do not grow, because for them $\lambda(q) < 0$.

The resultant picture of the coupled fields ζ_1 and n_1 is obtained by summation over all possible wave numbers of independent Fourier harmonics: $q_{max} \le q \le q_0$, where the value $q_{max} = (\lambda\sqrt{12}/ch)^{1/2}$ is determined from the condition of validity of the dispersion Eq. (4.39). At the characteristic values of λ, c, h, q_0 (see below) $q_{max}/q_0 \sim 10^{-4}$, and because of this the summation can be carried out in the limits $0 \le q \le q_0$:

$$\zeta_1 = N^{-1}\sum_{q \le q_0} A_q e^{iqx} + \text{c.c.},$$
$$n_1 = N^{-1}\sum_{q \le q_0} B_q e^{iqx} + \text{c.c.}, \quad (4.46)$$

where $N = L/2\pi h$, L is the length of the plate in the x-direction. We limit our consideration to the case of a sufficiently weak pump ($0 < R_v - \tau_v^{-1} \ll \tau_v^{-1}$). Then from Eqs. (4.43) and (4.46) we obtain (after integration) the resultant field of deformation in the form

$$\zeta_1 = (h^2/x\sqrt{6})(R_v\tau_v - 1)^{1/2}\sin(q_0 x). \quad (4.47)$$

The vacancy concentration field is given by

$$n_1 = C[\sin(q_0 x)(q_o^3/x - 12q_0/x^3 + 24/q_0 x^5) + \cos(q_0 x)(4q_0^2/x^2 - 24/x^4)], \quad (4.48)$$

where

$$C = R_v c^2 h^5 \rho q_0 (R_v\tau_v - 1)^{1/2}/(12\theta_v \tau_v^{-1}\sqrt{6}).$$

As is seen from Eqs. (4.47) and (4.48), the period of the quasilocalized periodic structure formed is equal to

$$d = 2\pi/q_0 = 2\pi\sqrt{D_\parallel \tau_v}\left(\frac{n_0}{n_{cr}} - 1\right)^{1/2}. \quad (4.49)$$

It follows from Eq. (4.49) and the expression for R_v (4.40) that the period of the structure increases with increasing h.

In the case of isotropic medium and uniform distribution of intensity in laser-beam cross-section, all directions of vector $\mathbf{q}$ are equivalent. The resultant field is obtained by substituting $\cos\mathbf{q}r = \cos(\mathbf{q}r\cos\varphi)$ in Eq. (4.46) instead of $\cos\mathbf{q}x$ and switching from summation over $\mathbf{q}$ to integration over $\mathbf{q}$ (r and φ are polar coordinates in the plane of the plate). Then, we have

$$\zeta_1 = 2hq_0(R_v\tau_v - 1)^{1/2} J_1(q_0 r)/(q_0 r\sqrt{6}), \quad (4.50)$$

$$n_1 = C[J_1(q_0 r)(q_0^3/r - 16q_0/r^3 + 64/q_0 r^5) + J_0(q_0 r)(4q_0^2/r^2 - 32/r^4)], \quad (4.51)$$

where $J_0(q_0 r)$ and $J_1(q_0 r)$ are the first-type Bessel functions of the zero and first order. One can easily check that expressions (4.47) and (4.48) for $x \to 0$ as well as the expressions (4.50) and (4.51) for $r \to 0$ remain finite. For axial symmetry of the laser field the center of the laser irradiated spot is the coordinates $r = 0$. The consideration given here remains valid if the spot radius $r_0 \gg d$. From Eqs. (4.50) and (4.51) one can see that the resultant fields of deformation and vacancy concentration are complicated concentric structures with a nonequidistant set of maxima, the magnitude of which decreases with the distance from the center of the spot.

Apart from the one-dimensional gratings and concentric rays, formation of the ray-star structures is also possible. Let us consider this case in detail.

Let the laser have Gaussian intensity distribution in the transverse cross-section of the beam given by Eq. (4.4). Then on the surface of the plate $z = h/2$ under the condition $h \ll r_0$ and with effective thermal run-

away from the surface $z = -h/2$ the stationary temperature distribution has the form

$$T(r) = T_0 \exp(-r^2/r_0^2).$$

Let us now find the stationary distribution of vacancy concentration assuming that generation of vacancies occurs due to the thermal mechanism. Under the conditions $r < r_0$ and $E_0 \equiv E_v \gg kT_0 t$ the stationary vacancy distribution is given by

$$\begin{aligned} n_0(r) &= \text{const} \exp(-E_v \exp(r^2/r_0^2)/kT_0) \\ &\approx n_0 \exp(-r^2/r_{\text{eff}}^2), \end{aligned} \tag{4.52}$$

where $r_{\text{eff}} = r_0(kT_0/E_v)^{1/2} \ll r_0$. Then, taking into account Eq. (4.52) one obtains the following equation for n_1:

$$\begin{aligned} \frac{\partial n_1}{\partial t} &= D_\parallel \Delta_\parallel n_1 - \tau_v^{-1} n_1 \\ -\theta_v \nu D_\parallel n_0 h (\Delta_\parallel^2 \zeta_1) &\exp(-r^2/r_{\text{eff}}^2)/2kT_0. \end{aligned} \tag{4.53}$$

In the derivation of Eq. (4.53) we neglected the dependence of T on r, because at $r < r_{\text{eff}}$ the function $T(r)$ varies little. Eq. (4.37) for ζ_1 remains unchanged. The solution of Eqs. (4.37) and (4.53) is developed in the form of radial rays:

$$\begin{aligned} \zeta_1 &= A\left(\frac{r}{r_{\text{eff}}}\right)^m \cos(m\varphi) \exp\left(-\frac{r^2}{r_{\text{eff}}^2} + \lambda t\right), \\ n_1 &= B\left(\frac{r}{r_{\text{eff}}}\right)^m \cos(m\varphi) \exp\left(-\frac{r^2}{r_{\text{eff}}^2} + \lambda t\right), \end{aligned} \tag{4.54}$$

where m is an integer. Substituting solutions in Eq. (4.54) into Eqs. (4.37) and (4.53) and assuming $r/r_{\text{eff}} \ll m$, we obtain the following expression for the growth rate of vacancy DDI with formation of radial rays

$$\lambda = R_v - D_\parallel \tilde{q}^2 - \tau_v^{-1}, \quad \tilde{q}^2 = 4(m+1)/r_{\text{eff}}^2, \tag{4.55}$$

where the value of R_v is given by Eq. (4.40).

The dispersion Eq. (4.55) is similar to Eq. (4.39) provided the substitution $q \to \tilde{q}$ is made.

To evaluate the number of rays in the structure we use $\tilde{q}^2 = q_0^2$, where q_0 is determined by Eq. (4.45). Then,

$$m \approx q_0^2 r_{\text{eff}}^2/4 = \pi^2 r_{\text{eff}}^2/d^2. \tag{4.55a}$$

Let us evaluate the critical concentration of vacancies according to Eq. (4.41). At $\rho = 5\,\text{g}\cdot\text{cm}^{-3}$, $c = 10^5\,\text{cm}\cdot\text{s}^{-1}$, $T_0 = 800$ K, $h \sim 10^{-2}$ cm, $K = 10^{12}\,\text{erg}\cdot\text{cm}^{-3}$, $a^3 \cong 10^{-22}\,\text{cm}^{-3}$, $|\theta_v| = Ka^3 \sim 10^{-10}$ erg, $\sigma = 0.3$, $D_\parallel \tau_v = l_v^2 = 10^{-5}\,\text{cm}^2$ from Eq. (4.41) we have $n_{\text{cr}} \sim 10^{18}\,\text{cm}^{-3}$. Note that with decreasing plate (film) thickness the critical value of vacancy concentration decreases $n_{\text{cr}} \sim h^2$.

At $n_0 = 1.1 n_{\text{cr}}$ from Eq. (4.49) we obtain the following expression for the period of the structure $d \sim 6 \times 10^{-2}$ cm. In the case of ray formation it follows from Eq. (4.27) that their number is $m \cong 10$ under the condition $d \lesssim r_{\text{eff}}$.

Evaluate now the characteristic time of vacancy DDI. From Eqs. (4.39) and (4.49) we have $\lambda_{\max}^{-1} = d^2/4\pi^2 D_\parallel \approx 10^2$ s, i.e., observation of the vacancy DDI is possible with the use of CW-lasers. Then, the condition of validity of the dispersion Eq. (4.39) $\lambda^2 \ll q^4 c^2 h^2/12$ reduces to the form $\sqrt{12} D_\parallel/ch \ll 1$, which evidently holds at the values of parameters used above.

The theory of vacancy DDI in thin plates and films developed above enables one to interpret the experimental results of the work [77], for which the formation of periodic concentric-ring and radial-ring (star) structures of deposits was observed in the deposition of Ni-ions from solution on the surface of thin ($h \sim 10^{-2}$ cm) metal plates, the other side of which was irradiated by a cw-laser with intensity of 10^4 - $10^3\,\text{W}\cdot\text{cm}^{-2}$. Note that due to heat conduction into the solution the condition of presence of temperature gradient along the z-axis was fulfilled, so that the distribution of vacancy concentration nonuniform along z was established, which is a prerequisite of the DDI with bending deformation (it can easily be seen from Eq. (4.33) that at $n_v(h/2) = n_v(-h/2)$ bending deformation does not occur). The above numeric estimates (as to the number of rays and period of ring structure) are close to the experimental observations of Ref. [77] (see Fig. 13 for comparison).

It is interesting to note that the "star"-structure was observed also in Ref. [78] in Ar^+-laser-induced chemical etching of Mo films on glass substrate. The number of rays increased with increasing laser power (Fig. 14), in accordance with the vacancy GDDI theory developed here.

4.3. Diffusion-Deformational Instability (DDI) on Semiconductor Surface

Now we consider the case in which the defect gratings are formed due to the self-consistent strain-induced defect fluxes along the surface of the semiconductor. We illustrate this phenomenon of the sequence of structural transformations at the surface of Si under irradiation by p-polarized millisecond laser pulses, and elucidate the nature of created structures in the solid and molten phases of the surface layer, and possibilities of controlling the structure geometry by changing the external control parameters [79].

4.3.1. Defect Grating Formation on Si Surface

The experimental studies in Ref. [79] were carried out with mirror polished surfaces of (111) and (100) monocrystalline silicon wafers with a thickness

$h = 0.5$ mm. The Nd : YAG laser which provided pulses of polarized output radiation at $\lambda = 1.06$ μm with pulse energy W up to 3 J and pulse duration $\tau_p = 1.6$ ms was used for surface irradiation. The p-polarized laser radiation was focused on the surface of the Si wafer to a spot diameter $r_0 = 1.2$ mm. The diagnostics of surface changes with the help of recording of thermal radiation, probe-beam specular and diffraction reflection enabled one to follow the dynamics of development of the ordered structures in solid and molten phases. The irradiated samples were also studied with optical and electronic microscopes, and a profilometer.

Surface irradiation was performed as follows: laser fluence at the surface of the Si wafer was increased stepwise from $\Phi_L = 7.0$ J·cm^{-2} to $\Phi_L = 95.5$ J·cm^{-2}, the sample being shifted perpendicular to the incident laser beam after each laser shot, thus ensuring irradiation of fresh surface area. Experiments were carried out both in atmosphere and in a vacuum.

We focus here only on those experimental findings of Ref. [79] which pertain to the discussed problem of defect grating formation. The irradiated samples were studied with a microscope and a profilometer. At a normal incidence of the excitant laser beam and at laser energy fluences up to $\Phi_L = 8.5$ J·cm^{-2} no changes in surface morphology were observed. Increase of laser fluence over 8.5 J·cm^{-2} caused formation of a cell-like structure. Every cell was either a melted square (in the case of the (100) surface symmetry) or triangle (for (111) surface symmetry) (on the photograph the cells are seen as points – see Fig. 15a). In the range of fluences $\Phi_L = 8.5$ - 25 J·cm^{-2} the cells in the irradiated spot were distributed randomly, but the sides of the cells were all oriented along the crystallographic directions. With fluence increase we observed a rise in the cell size, and secondly, the cells were ordered forming a two-dimensional cell structure (or two-dimensional grating); with period $d_1 = 3$ - 3.5 μm (see Fig. 15a), laser fluences $\Phi_L = 25$ J·cm^{-2} the average cell size was about 1 - 3 μm and the cells completely covered the irradiated area. Orientation of the two-dimensional grating did not depend on laser radiation polarization. However, further evolution of the two-dimensional grating of cells with the increase of fluence in the range $\Phi_L = 25$ - 34.5 J·cm^{-2} depended on relative orientation of crystallographic axes and vector of polarization of laser radiation.

Thus, when the electric field amplitude **E** of the laser radiation was oriented along one of the crystallographic axes of the surface (100), increase of the number density of cells (and their fusion) in a direction perpendicular to this axis (see Fig. 15b) was observed. Thus, in this case a "one-dimensional" grating with period $d_1 = 3$ - 3.5 μm, oriented perpendicular to the crystallographic axis mentioned above and electric field **E**, was formed at the surface. When the electric field **E** did not coincide with any of the crystallographic axes, similarly, two gratings were formed oriented perpendicularly to the crystallographic axes of the surface with period $d_1 = 3$ - 3.5 μm (see Fig. 15a). Studies of the transverse cut with an electron microscope showed that gratings with a period d_1 are formed due to surface relief modulation with an amplitude of about 2×10^{-5} cm.

When the laser radiation was incident on the surface at an angle α, the formation of surface structures described above was also observed at corresponding laser fluences, their period being independent of the angle of incidence and being equal to $d_1 = 3$ - 3.5 μm as in the case of normal incidence. However in this case, apart from the structures just described, a new type of grating started to appear with a period given by a well-known expression [22 - 26]:

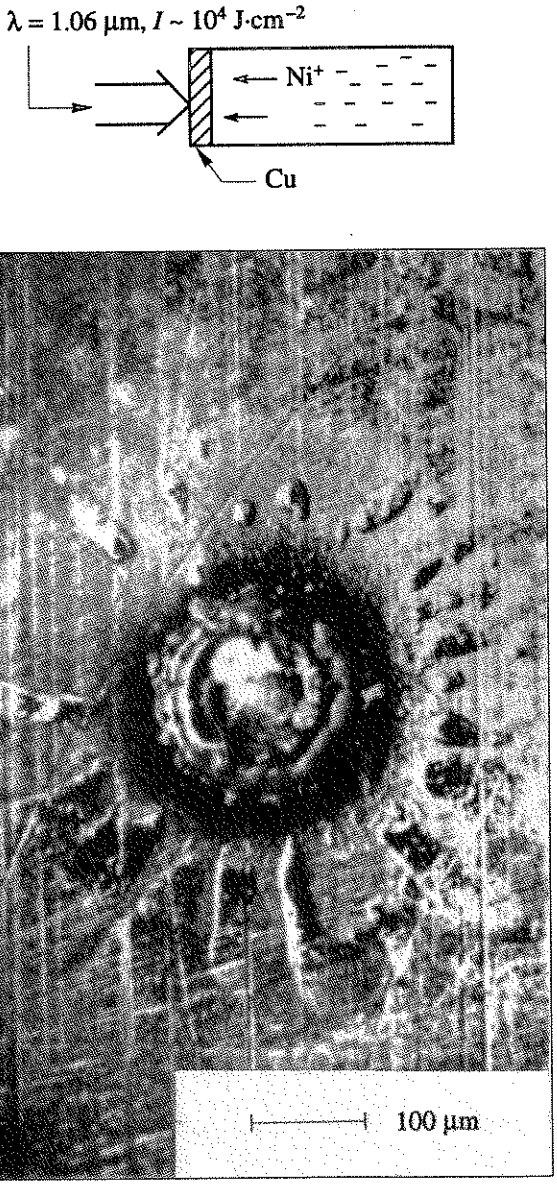

Fig. 13. *Star structure of Ni deposit formed in laser deposition from solution [77]. In the inset the experimental arrangement is shown. The "star"-structure of the deposit is formed on the inside face of the Cu plate.*

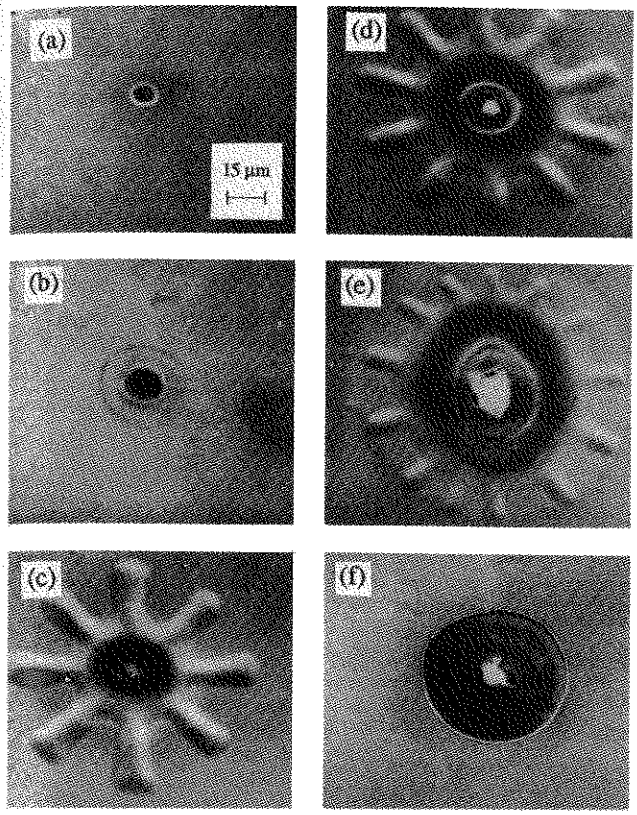

Fig. 14. *Scanning electron micrographs of ray-star structures etched into Mo / glass film by means of Ar^+ laser irradiation ($2r_0 = 16$ μm). P = 10 mW (a), 20 mW (b), 50 mW (c), 100 mW (d), 500 mW (e), 150 mW (f) [78].*

$$d_2 = \frac{\lambda}{1 - \sin\alpha},$$

λ is radiation wavelength and oriented perpendicular to the laser electric field **E**. When vector **E** coincided with one of the crystal axes, two gratings with a similar orientation perpendicular to **E** were observed at the surface, with the period of one of them being independent of the angle of incidence and equal to $d_1 = 3 - 3.5$ μm, and the period of the other varying depending on the angle of incidence. When the vector **E** did not coincide with the crystal axis a complicated superposition of three gratings was observed, that is, two gratings with period d_1 oriented perpendicular to the crystallographic axes and one grating with period d_2 oriented perpendicular to **E** (see Figs. 15b, 15c). It should be noted that at normal incidence of the laser beam, gratings with a constant period d_1 dominated, while the gratings with a period d_2 dependent on the angle of incidence were weak. With increase of the incidence angle the "contrast" of gratings with a constant period d_1 rapidly decreased and at $\alpha = 30°$ gratings with angle-dependent period d_2 dominated (see Fig. 15d). Similar studies were also carried out in a vacuum at 10^{-2} torr. The results obtained were qualitatively the same as those obtained in air.

Obviously, the grating with a period and rulings perpendicular to the electric field vector **E** of the laser field is the interferential (*I*) grating [22 - 26], usually created under the influence of *p*-polarized laser radiation sufficiently intense to cause melting of a thin surface layer. Similar *I*-gratings have been observed at other durations of laser pulses. Thus, dynamics of formation of *I*-structures at the surface of Si under excitation by a nanosecond laser pulse (≈ 1.06 μm) were studied in Ref. [22]. Diagnostics of surface changes were performed by using mirror reflectivity and diffraction of the probe pulse. Similar studies were carried out with microsecond pulses (λ = 10.6 μm) [80]. Periodic structures observed in these studies were of interference origin and are well understood.

Gratings and cell structures with a period independent of the angle of incidence are the most interesting. Creation of cell structure at the surface of Si was observed earlier in a number of experiments. It is well established that these structures are formed due to local melting of the surface. However, the nature of these structures as well as that of quasiperiodic local melting under laser excitation of semiconductors currently remain under study.

We attribute the appearance of lattices with a period d_1 to generation and ordering of defects in a thin (of the order of 10^{-5} cm) surface layer of a semiconductor. Laser excitation leads to generation of a great number of point defects (vacancies and interstitials in the near surface layer with thickness of the order of 10^{-5} cm) (Sec. 3). The spatially uniform field of point defects with concentration n_{d0} becomes unstable as the latter exceeds a certain critical value $n_{d0} > n_{cr}$, and diffusion-deformational instability develops, leading to formation of either extended defects (voids or dislocation loops) (Sec. 5) or periodic gratings of point defect accumulations.

The mechanism of DDI is similar to that considered in Sec. 4.2. The fluctuating harmonic of defect concentration gives rise to the appearance of a harmonic of surface deformation. Because a defect in the field of deformations possesses energy (Eq. (1.1)), there appear defect fluxes directed toward deformation potential wells. This causes gain of the initial amplitude of the seed Fourier harmonic of defect concentration and development of the instability. As a result, defects are self-localized at deformational potential wells which they themselves created. DDI is stabilized by nonlinearity of the elastic continuum (Sec. 4.2). Thus, according to the concept of DDI, two scenarios for grating formation with a period d_1 are possible:

(1) deformation-induced point defect condensation with formation of dislocation loops (Secs. 5.1 and 5.2) and subsequent self-consistent deformation-induced redistribution of the loops either by glide (Sec. 7.1) or by climb (Sec. 7.2) accompanied by formation of periodic gratings of dislocations;

(2) formation of periodic point defects accumulates with subsequent possible creation of dislocation loops in those piles. Consideration of the dislocation-defor-

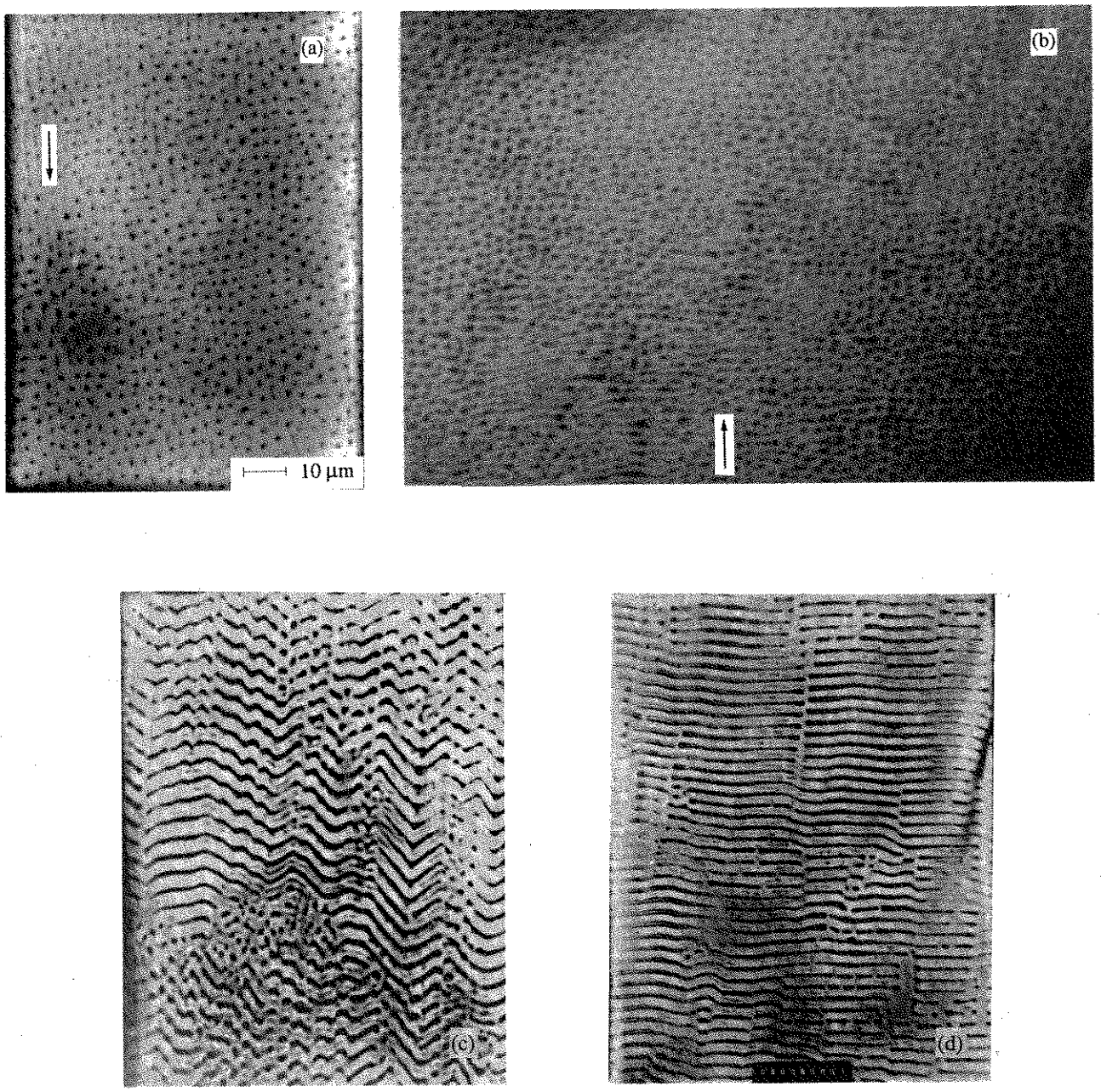

Fig. 15. *Photographs of laser-irradiated Si (100) surface. The direction of the x-axis (pointer) coincides with one of the crystallographic directions. $\alpha = 0°$. The electric field vector **E** is directed at an angle of 45° with respect to the x-axis. Two-dimensional cell structure is observed (a); $\alpha = 0°$, $\mathbf{E} \parallel x$. The grating with $d_1 = 3.5$ μm and rulings perpendicular to **E** appears (b); $\alpha \equiv 30°$, **E** is directed at an angle of 45° with respect to the x-axis. Superposition of three gratings, two with $d_1 = 3.5$ μm oriented perpendicular to the crystallographic axes, and one with the period d_2 dependent on incidence angle and oriented perpendicular to the vector **E** (c); $\alpha = 45°$ (d). One-dimensional grating with a period d_2 depending on the incidence angle.*

mational instability (Sec. 7) shows that the processes of dislocation self-organization are too slow and can be neglected on a time scale of 10^{-3} s, thus only the second scenario seems to fit the experimental findings of Ref. [79].

Local deformation caused by local accumulation of defects causes decrease of the melting temperature [81], so that at sufficiently high laser intensity the gratings of defects manifest themselves by the onset of local melting (Sec. 5.3.2). Note that, as predicted by the theory of DDI (see Sec. 4.3), when the surface grating of defects is formed even without melting, the surface relief becomes periodically modulated, the defects being accumulated either at minima (vacancies) or at maxima (interstitials). However, the amplitude of relief modulation is small ($h \sim 10^{-5}$ cm) and is less than the amplitude of the relief $H > 10^{-5}$ cm appearing as a result of inhomogeneous melting. The

theory of periodic grating formation consisting of laser-induced defects (vacancies and interstitials) as a result of development of DDI is described in Sec. 4.3.1. It is shown that the main experimental features as to the period and orientation of gratings with a period obtain a theoretical account within the framework of this model.

The model of DDI taking into account point defects explains, in particular, variation of grating orientation with a period when orientation of the **E** vector of a sufficiently strong laser field changes with respect to the crystallographic axes. In fact, in a weak field **E**, deformation-induced point defect fluxes are directed primarily along distinguished crystallographic directions (at the (100) surface the latter are perpendicular to each other) due to anisotropy of elastic coefficients. Hence two orthogonal gratings are formed in this case. Crossing of these two gratings forms a cell structure of defect accumulations which is revealed by local melting (Fig. 15a).

A sufficiently strong laser field with the vector **E** oriented along one of the crystallographic directions breaks covalent bonds along this direction and thus violates the symmetry of deformation-induced fluxes of point defects (see Sec. 4.3.3); as a result, the two-dimensional grating (Fig. 15a) is transformed into a one-dimensional grating (Fig. 15b). If vector **E** of a strong laser field with intensity close to the melting threshold is oriented at an angle of 45° with respect to the crystallographic axes, then the symmetry of point defect fluxes is restored and there must appear a two-dimensional grating with a period, and moreover, an ordinary *I*-grating with a period and rulings perpendicular with respect to **E**, which is in fact observed in experiment (see Fig. 15c). The DDI theory quantitatively predicts also the period d_1 of the defect-deformational gratings, as well as characteristic time of their formation (see Sec. 4.3.2).

Lastly the fact that at $\alpha > 30°$ the only grating left on the surface is an *I*-grating with period d_2 is explained by the influence of the *I*-grating on the formation of defect grating with period d_1. In fact the interference light field, spatially periodic along the surface, leading to *I*-grating formation (see the discussion in Sec. 2.6 and Refs. [22 - 26]) gives rise to periodic surface temperature and hence strain fields. This brings about periodic forces acting on the defects and resultant periodic defect fluxes tending to redistribute the defects and to form a defect surface grating with period d_1. When $d_1 \ll d_2$ these periodic forces are averaged out and mutually cancel, so that a defect grating with DD-period d_2 is formed. On the contrary when $d_1 > d_2$ the spatially oscillating strain field with period d_1 entrains defects into periodic potential wells forming a defect grating with the same period d_1. Thus the condition $d_1 \approx d_2$ is the critical condition of disappearance of d_2 grating, i.e., the angle of incidence must exceed the critical value

$$\alpha > \alpha_{cr} \cong \text{asin}\,(1 - \frac{\lambda_L}{d_2}) .$$

At $\lambda_L = 1$ μm, $d_2 = 3.5$ μm we have that the d_2-grating disappears at $\alpha \approx 30°$, which in fact is recorded in experiments of Ref. [79]. This hypothesis of defect entrainment by interference surface light field needs further experimental investigation.

Thus, from the point of view of the DDI model implying defect ordering the main features of Si surface morphology changes remaining after excitation by linearly polarized laser radiation and seen by microscope are quite explainable. Let us proceed to the exposition of quantitative theory of defect-deformatinal grating formation at semiconductor surfaces under laser irradiation.

4.3.2. "Film-on-Substrate" Model of Surface DDI

We assume here that a high concentration of point defects (vacancies (d = v) or interstitials (d = i)) is created in the near surface layer of a semiconductor under laser irradiation. As was shown in Sec. 3 the high values of point defect concentration can be achieved as a result of simultaneous action of three factors: reduction of energy required for formation of new defects by approximately an order of magnitude due to local electronic excitation near earlier created defects, laser-induced heating, and deformation of the surface layer. The thickness h of the subsurface layer, in which enhanced defects generation takes place was determined in Ref. [54]. It was found that the value of h, 60 - 100 nm is less than the optical absorption length and is determined by the initial material defectiveness. It will be assumed here that, according to Ref. [54], the thickness of the laser-induced defect enriched layer h is also determined by the material destructivity and amounts to about 10^{-5} cm.

The defect enriched layer will be considered here as a film of thickness h with density ρ_f and Young's E_f module, and the rest of the semi-infinite crystal as a substrate with parameters ρ, E with which the film is tightly bonded. Let the plane $z = 0$ be the interface plane between the film and the substrate, and the z-axis be directed inside the crystalline substrate (Fig. 16). There are two equivalent orthogonal crystallographic directions at the (100) surface of Si. Let the x-axis be along one of these directions and the y-axis be along the other.

It will be assumed here that the diffusion coefficient of defects along the surface (or along the film) D_d is much larger than that into the bulk, $D_d \gg D_z$, which is usually the case. Then defects are redistributed only along the film, and one can write

$$n_d(x, y, z, t) = n_d(x, y, t) \exp(-\gamma_d (z + h)) . \quad (4.56)$$

Here the constant quantity γ_d is determined by the initial processes of point defect creation and governs the thickness of the defect enriched surface layer. Thus, it will be supposed here that $\gamma_d = h^{-1}$. The equation for defect concentration has the form

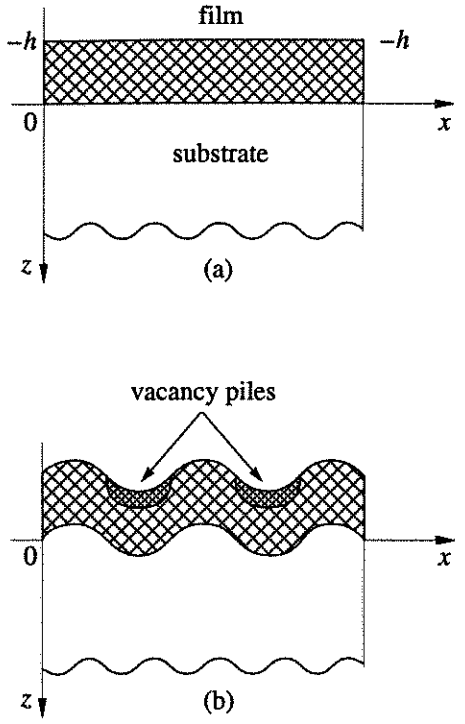

Fig. 16. *A model of the film-on-substrate. Defects are homogeneously distributed along x, the film is non-deformed (a); formation of coupled gratings of bending deformation and concentration of defects (b).*

$$\frac{\partial n_d}{\partial t} = D_d \Delta_{\parallel}(n_d) - \frac{1}{\tau_d} n_d - \frac{D_d \theta_d}{kT} \mathrm{div}_{\parallel}(n_d \mathrm{grad}_{\parallel}(\mathrm{div}(\mathbf{U}_f))), \tag{4.57}$$

$\mathbf{U}_f$ is the medium displacement vector in the film and subscript $\parallel$ indicates the differentiation in respect to x and y. Deformation of the surface layer (or film) is described by the bending coordinate ζ. This coordinate satisfies the equation

$$\frac{\partial^2 \zeta}{\partial t^2} + c_f^2 l_0^2 \Delta_{\parallel}^2(\zeta) + f_{NL}(\zeta) = \frac{\sigma_{\perp}}{\rho_f h}, \tag{4.58}$$

here $c_f^2 = E_f(\rho_f(1-\sigma_f^2))^{-1}$, σ_f is the Poisson coefficient of the film, $\sigma_{\perp}$ is stress normal to the film, f_{NL} is the term describing film bending nonlinearity (cf. Eq. (4.33)). Film bending is related to compression-stretching deformation of the film

$$\mathrm{div}(\mathbf{U}_f) = -\nu_f(z + h/2)\Delta_{\parallel}\zeta, \tag{4.59}$$

where $\nu_f = (1-2\sigma_f)/(1-\sigma_f)$.

Moreover, film bending is also related to elastic deformation of the surface of the substrate which is governed by the equation for the displacement vector of the elastic continuum of the substrate

$$\frac{\partial^2 \mathbf{U}}{\partial t^2} = c_t^2 \Delta \mathbf{U} + (c_l^2 - c_t^2)\,\mathrm{grad}\,\mathrm{div}\,\mathbf{U} + F_{NL}(\mathbf{U}). \tag{4.60}$$

The term F_{NL} describes nonlinearity of the elastic continuum. At the film-substrate interface we have the following boundary conditions.

Displacement along the z-axis must be continuous at $z = 0$, hence

$$U_z|_{z=0} = \zeta. \tag{4.61}$$

Tangential stress due to defects in the film must be compensated for by tangential (shear) stress developed in the substrate at $z = 0$. Hence, taking into account Eq. (4.56), we have

$$\mu\left(\frac{\partial U_{x_\alpha}}{\partial z} + \frac{\partial U_z}{\partial x_\alpha}\right) = \theta_d \frac{\partial}{\partial x_\alpha}\int_{-h}^{0} n_d(x, y, z)\,dz \cong \theta_d h \frac{\partial}{\partial x_\alpha}(n_d(x, y)), \tag{4.62}$$

where $n_d(x, y)$ is the defect concentration at the surface, $x_\alpha = \{x, y\}$, and μ is the shear modulus of the substrate.

Stress normal to the plane $z = 0$ determines $\sigma_{\perp}(x, y)$ in the film

$$\left(\frac{\partial U_z}{\partial z} + (1-2\beta)\left(\frac{\partial U_x}{\partial x} + \frac{\partial U_y}{\partial y}\right)\right)\Big|_{z=0} = \frac{\sigma_{\perp}(x, y)}{\rho c_l^2}; \quad \beta = c_t^2/c_l^2. \tag{4.63}$$

Displacement along the x and y directions at the boundary $z = 0$ can be neglected, because for example

$$U_x|_{z=0} = -\frac{h\partial\zeta}{2\partial x} \sim -\frac{hq}{2}\zeta = -\frac{h\pi}{d_1}\zeta, \tag{4.64}$$

where d_1 is the period of the defect structure formed under DDI (see below). Because under bending DDI in a film the condition $(h\pi)/d_1 \ll 1$ holds, it is seen from Eq. (4.64) that $U_x \ll U_z$, so that displacement along x (and similarly along y) can in fact be neglected.

The set of Eqs. (4.57 - 4.63) is a closed set describing DDI in a surface layer containing defects. We limited our analysis here to consideration of only the linear stage of DDI (or stability analysis of Eqs. (4.57 - 4.63)). This enabled us to determine the threshold of DDI, geometry and period of the DD structures and characteristic time of their development.

Later on we shall limit our consideration to DDI in the one-dimensional case, where defects are redistributed only along one crystallographic direction x. We seek the solution of the set of linearized Eqs. (4.63 - 4.65) in the form

$$n_d = n_{d0} + N\exp(iqx + \lambda t), \quad \zeta = A\exp(iqx + \lambda t), \tag{4.65a}$$

$$\sigma_{\perp}(x) = \sigma_{\perp}\exp(iqx + \lambda t). \tag{4.65b}$$

$$U_x = (-iqBe^{-\kappa_t z} - i\kappa_t Ce^{-\kappa_t z}) \exp(iqx + \lambda t),$$
$$U_z = (\kappa_t Be^{-\kappa_t z} + qCe^{-\kappa_t z}) \exp(iqx + \lambda t), \quad (4.65c)$$

where n_{d0} is the spatially homogeneous distribution of defects n at the surface. The solution in this form contains seven unknown quantities: A, B, C, N, $\sigma_\perp$, q, and λ. The expression for the components of the displacement vector in the substrate is similar to the free part of the displacement vector under EDTI (cf. Eq. (2.18)) and both are the analogies of the displacement vector $\mathbf{U}$ in the surface acoustic (Relay) wave (see Ref. [76]).

From Eqs. (4.57 - 4.63), using Eq. (4.65), one obtains six homogeneous algebraic equations for determining the seven unknown quantities listed above (for details see Ref. [79]). Thus, the set of Eqs. (4.57 - 4.63) permits one to find the dependence $\lambda = \lambda(q)$. If the condition $\lambda^2 / c_{t,l}^2 \ll q^2$ holds (this limit can be taken only at the end of all calculations) for the growth rate of DDI one obtains

$$\lambda = -(D_d q^2 + \tau_d^{-1}) + D_d q h^{-1} \frac{6E(1-2\sigma)\theta_d^2 n_{d0}}{E_f(1-\sigma^2)(1-2\sigma)kT\mu}. \quad (4.66)$$

Eq. (4.66) is derived from a more general expression of Ref. [79] under the condition

$$\rho_f c_f^2 q^3 h^3 / 12\rho c_t^2 > 2(1-\beta)$$

(this condition holds under assumptions made). For clearer presentation of the results obtained let $E = E_f$, $\sigma = \sigma_f$, and take into account that $\sigma \ll 1$.

Then from Eq. (4.66) we obtain finally the following expression for the DDI growth rate

$$\lambda = -(D_d q^2 + \tau_d^{-1}) + D_d q h^{-1} \frac{6\theta_d^2 n_{d0}}{\mu kT}. \quad (4.67)$$

The dependence $\lambda = \lambda(q)$ is plotted in Fig. 17. The maximum value λ_{max} is achieved at $q = q_{max}$

$$q_{max} = h^{-1} \left(\frac{|\theta_d|}{kT}\right) \left(\frac{3|\theta_d| n_{d0}}{\mu}\right). \quad (4.68)$$

The maximum growth rate value is equal to

$$\lambda_{max} = D_d q_{max}^2 - \tau_d^{-1}. \quad (4.69)$$

An instability appears at $\lambda_{max} > 0$, that is, when the spatially homogeneous defect concentration exceeds a critical value n_{dcr} obtained from Eq. (4.69)

$$n_{d0} > n_{dcr} = \frac{h}{\sqrt{D_d \tau_d}} \frac{kT\mu}{3\theta_d^2}. \quad (4.70)$$

Note that DDI appears at any sign of θ_d ($\theta_d < 0$ for vacancies and $\theta_d > 0$ for interstitials).

At characteristic values of the parameters $h = 10^{-5}$ cm, $T = 1.5 \times 10^3$ K, $\mu = 10^{12}$ erg·cm^{-3}, $|\theta_d| = 10^2$ eV, $D_d = 10^{-5}$ cm^2·s^{-1}, $\tau_d = h^2 D_d^{-1} \approx 10^{-5}$ s from Eq. (4.70) one finds that the critical defect concentration is $n_{dcr} = 10^{19}$ cm^{-3}. Thus, the development of DDI at the surface leads to formation of a grating of defect concentration (Eq. (4.65a)) and grating of bending deformation coupled to it (Eq. (4.65b)), the grating period being equal to

$$d_1 = \frac{2\pi}{q_{max}} = h \frac{kT\mu}{3|\theta_d|^2 n_{d0}}. \quad (4.71)$$

At the same values of parameters as those used when estimating (4.70) and at $n_{d0} = 3 \times 10^{19}$ cm^{-3} (which is an order of magnitude larger than the critical value (4.70)) one obtains the defect-deformational grating period value $d_1 = 3 \times 10^{-4}$ cm, which is in agreement with the experimental results of Ref. [79] (see Fig. 15). Note the important peculiarities of the obtained results.

(1) The time of surface defect grating formation, t_d, is determined from the expression which can be derived from Eqs. (4.68) and (4.69)

$$t_d \cong \lambda_{max}^{-1} = \frac{\tau_d}{n_d^2 / n_{dcr}^2 - 1}. \quad (4.72)$$

Thus, near the threshold ($(n_d^2/n_{dcr}^2 \to 1) t_d \to \infty$) (critical slowing down typical of phase transitions); at large excesses of the threshold ($n_d^2/n_{dcr}^2 \gg 1$)

$$t_d = (D_d q_{max}^2)^{-1}. \quad (4.73)$$

At $D_d = 10^{-5}$ cm^2·s^{-1}, $q_{max} = 2\pi / d_1$ and $d_1 = 3 \times 10^{-4}$ cm one obtains from Eq. (4.73) that the defect-deformational grating formation time is $t_d = 2 \times 10^{-4}$ s. Consequently the grating has time to develop during the millisecond laser pulse.

(2) The surface grating period is proportional to the film thickness $d_1 \sim h$. This characteristic feature of DDI with bending deformation in films takes place also in the theory of boundary formation under laser-induced recrystallization of thin semiconductor films on substrates (Sec. 4.4) and under formation of surface dislocation gratings (Sec. 7).

It is interesting to note that the one-dimensional gratings of surface relief are formed under ion implantation of the Si surface [107]. The periods of these gratings ($d \sim 0.5$ - 10 μm) are proportional to the thickness of the implanted layer h in accordance with the theory of DDI developed in this section.

(3) Since $n_{d0} \sim \exp(-E_{eff} / kT)$, where E_{eff} is the effective energy of defect formation (renormalized by laser excitation, (see Sec. 3), from Eq. (4.71) one obtains $d_1 \sim T\exp(E_{eff} / kT)$, that is, the grating period rapidly decreases with increase in temperature.

(4) From Eqs. (4.65a) and (4.65b), and the results of Ref. [79] we obtain that the ratio of amplitudes of the surface grating of defect concentration and of bending deformation of a film is equal to

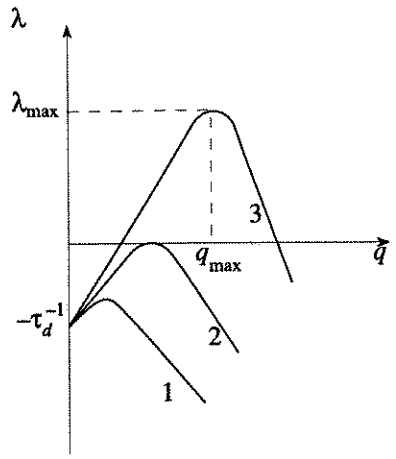

Fig. 17. *Growth rate of the DDI as a function of the wave number q of the grating: (1) – $n_{d0} < n_{d\,cr}$; (2) – $n_{d0} = n_{d\,cr}$; (3) – $n_{d0} > n_{d\,cr}$*

$$\frac{n_d}{\zeta} = \frac{N}{A} = |\text{const}|\,\text{sgn}\,d, \tag{4.74}$$

where $|\text{const}| > 0$. This means that vacancies ($\text{sgn}(d) < 0$) are accumulated at the surface relief minima (where $\zeta > 0$) (see Fig. 16), while interstitials, on the contrary, are accumulated at surface relief maxima.

(5) If the x and y directions are both equivalent and preferred, that is, frequency of elementary jumps of defects while migrating along the x or y direction is much higher than along other directions, then DDI must lead to formation of the two-dimensional grating of defects and bending deformation given by formulas similar to Eq. (4.65)

$$\begin{aligned} n_d(x, y) &= N\exp(\lambda t)\cos q_{\max}x\cos q_{\max}y \\ \zeta(x, y) &= A\exp(\lambda t)\cos q_{\max}x\cos q_{\max}y, \end{aligned} \tag{4.75}$$

where $q_{\max}$ and the period d_1 are given by Eqs. (4.68) and (4.71).

(6) We considered a linear regime of DDI-exponential growth of surface grating amplitudes in time. DDI stabilization occurs due to nonlinearity of the film bending deformations (the term f_{NL} in Eq. (4.58)) or due to nonlinearity of the elastic continuum (the term F_{NL} in Eq. (4.60)). If elastic nonlinearity is taken into account one can describe the stationary state of the bending deformation grating and defect concentration grating coupled to it. Although this nonlinear problem has not yet been solved in the present "film-on-substrate" model, the nonlinear solution for unsupported film (Sec. 4.2) enables one to envisage that the amplitude of the surface periodic relief is of the order of or less than h.

We note that in this state the defects are trapped in potential strain wells with high diffusion barriers, so that $D_d \to 0$. Since $\tau_d = l_d^2 / D_d$, where l_d is the mean distance between the defect sinks, then $\tau_d \to \infty$, and this state in fact is stationary.

Let us now discuss the question of when one can expect the formation of one-dimensional or two-dimensional gratings with the period d_1 under the action of a strong linear polarized laser beam.

4.3.3. Control of Defect Flux Direction by Linear Polarized Laser Light

Let linearly polarized laser radiation be incident on a surface (100) of a covalent semiconductor (Si) at an angle α, and $\mathbf{E}_t$ be the electric field component along the medium surface (see Fig. 18). Arrangement of atoms in an elementary cell of Si, which are bound by covalent bonds, is shown in Fig. 18a. The elementary cell with an introduced defect (interstitial i) is shown from above in Fig. 18b. If the electric field vector $\mathbf{E}_t$ is directed as shown in Fig. 18 the field interacts only with electron bonds $2 == 1$, $1 == 4$ and does not interact with bonds $3 == 1$ and $1 == 5$. In a sufficiently strong laser field the number of excited bonds directed as $2 == 1$ is expected to be large. It is important that excitation of bonds will take place primarily in a vicinity of defects which renormalize locally (reduce) by their elastic field the electronic transition frequency from the upper to lower state of a covalent bond (or from valence band to conduction band). Electron transition from lower, bonding state to upper, antibonding state signifies bond breaking.

Suppose that the laser-induced breaking of bonds $1 == 2$, $1 == 4$ occurs in a vicinity of the interstitial, while the bonds $3 == 1$ and $1 == 5$ remain nonexcited (see Fig. 18b). This means that force constants of interatomic bonds K_{12} and K_{14} tend to zero ($K_{12} \approx 0$, $K_{14} \approx 0$), and force constants K_{31}, K_{15} retain their initial values. The probability of a defect (interstitial or vacancy) jump from one equilibrium state to another via a saddle point (atom 1) (see Fig. 6b) along the $4 == 1 == 2$ direction is

$$K_{412} = \nu\exp(-H_{41}/kT), \tag{4.76}$$

where $\nu = \text{const}$ and the activation energy of the jump is determined by the force constant K_{41} [82]

$$H_{41} = \frac{K_{14}a^2}{6\pi^2}. \tag{4.77}$$

When the bond $1 == 4$ is excited the activation energy $H_{41} \to 0$, and jump probability along the $4 == 1 == 2$ direction becomes much higher than jump probability along the direction $3 == 1 == 5$, because the quantity H_{31} remains unchanged ($K_{315} = \nu\exp(-H_{31}/kT)$).

Thus, under excitation by sufficiently strong laser radiation linearly polarized along one direction of bonds, there appears asymmetry in probability of elementary jumps in a vicinity of a defect: jump probability along the electric field vector $\mathbf{E}_t$ is higher than along a perpendicular direction.

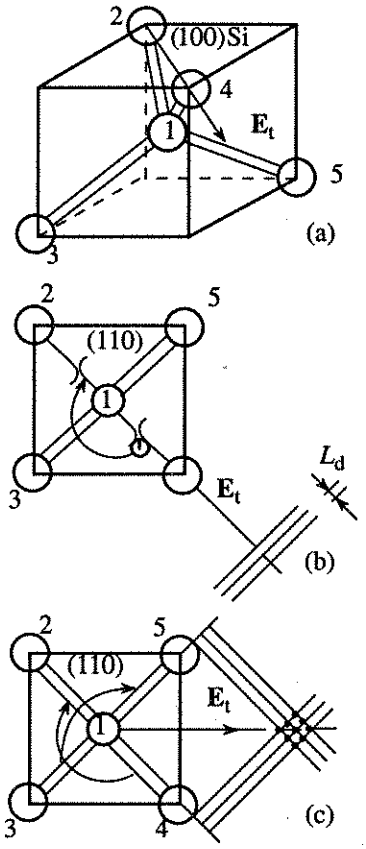

Fig. 18. *Controlling elementary jumps of a point defect in Si by means of a linearly polarized laser field. Atoms with covalent bonds in a cell (a); plane (100) viewed from above. The vector E_t is directed along the 2 == 1 == 4 bonds. Bonds 2 == 1 and 1 == 4 are broken by excitation with the field E_t. The pointer shows the direction of dominating jumps of a defect (one-dimensional grating formation) (b); vector E_t is directed at an angle of 45° with respect to the bonds. A two-dimensional cell structure of defects is formed (c).*

When describing defect migration in terms of diffusion this means that there appears laser-induced diffusion asymmetry, namely, defect diffusivity in a direction of $\mathbf{E}_t$ (along the 4 == 1 == 2 bonds) is larger or much larger than diffusivity in a perpendicular direction. Under development of the above described DDI the asymmetry of diffusivity coefficients must lead to formation of a one-dimensional grating of defects with rulings perpendicular to $\mathbf{E}_t$ (see Fig. 6b). It is seen from Fig. 18c that when the electric field $\mathbf{E}_t$ is directed at an angle of 45° with respect to the bonds 4 == 1 == 2 and 3 == 1 == 5, symmetry of diffusion along these directions is restored, so that a two-dimensional DD grading of defects must appear as a result of DDI. These conclusions are in agreement with experimental observations described in Sec. 4.3.1.

In summary, the theory of point defect DDI developed in this section satisfactorily describes the main experimental data on laser-induced generation and control of surface gratings at the surface of Si. Agreement between experimental data and predictions of the theory enabled us to conclude that the process of point defect ordering accompanied by formation of the defect-deformational gratings revealed by inhomogeneous melting is responsible for surface relief grating formation with a period $d_1 \approx 3$ μm independent of incidence angle.

4.3.4. Electron DDI on the Surface of a Semiconductor

The results obtained in Sec. 4.3.2 are valid also if one considers the electron-hole pairs as a defect subsystem. In this case $n_d = n_e$ is concentration of e-h pairs and the defect-elastic continuum interaction energy is again given by Eq. (1.1). Thus all the formulas obtained in Sec. 4.3.2 remain valid for the case of e-h pairs if one puts $h \sim \gamma_0^{-1}$ where γ_0 is optical absorption coefficient (we assume that during the time of electron DDI development t_e the electron diffusion length $(D_e t_e)^{1/2} < \gamma_0^{-1}$ where D_e is electron diffusion coefficient).

As a result of electron DDI development the surface grating of electron concentration and strain (Eq. (4.65)) with the period (Eq. (4.71)) arises. The electron DDI occurs under exceeding of the critical concentration of e-h pairs – (Eq. (4.70)). In these expressions $\theta_d = \theta$ is now the interband deformation potential. On the (100) surface two orthogonal gratings of electron concentration must be generated, the intersection of which forms the cell surface structure. The periodic increase of surface electron concentration leads to periodic increase of surface temperature and resultant periodic surface damage, i.e., to formation of surface cell structure.

Let us evaluate the critical concentration of e-h pairs, the period of electron DD structure and the time of electron DDI development.

For the critical concentration of e-h pairs from Eq. (4.70) we have

$$n_{ecr} = \frac{h}{(D_e\tau_e)^{1/2}}\frac{\mu kT}{3\theta^2} \sim 3\times10^{19}\,\mathrm{cm}^{-3}$$

at $h \sim \gamma_0^{-1} \sim 10^{-5}$ cm, $D_e \sim 10$ cm^2·s^{-1}, $\tau_e \sim 10^{-9}$ s, $\theta \sim 10$ eV, $\mu \sim 10^{12}$ erg·cm^{-3}, $kT \sim 0.1$ eV, i.e., at temperature close to melting. Such concentration can be achieved under the action of powerful picosecond laser pulses.

For the time of electron DDI development from Eq. (4.72) we obtain under the condition of strong exceeding of the threshold

$$t_e = \tau_e\left(\frac{n_{ecr}}{n_{e0}}\right)^2.$$

Thus the electron DDI develops during a time much less than the time of electron-hole recombination τ_e.

For the period of cell structure (grating) we have from Eq. (4.71) at $n_{e0} = 3n_{ecr}$

$$d_1 \cong 2\ \mu\mathrm{m}.$$

Formation of two-dimensional surface structure of cells in the form of evaporation craters was observed on Ge surface under irradiation by powerful picosecond pulses of an Nd : Yag laser in Ref. [38].

The time of formation of this structure was 10^{-10} s, i.e., it was formed after the end of a laser pulse. The characteristics of electron surface DDI as regards time of development, critical concentration and structure period correspond well to the experimental findings of Refs. [38, 71].

4.3.5. Metastability of Defect-Deformational Structures

We will show now that the periodic or localized DD structures formed due to the GDDI development are metastable or stable states of the material, appearing due to the phase transition of the second kind.

For this aim we consider the free energy density of the coupled elastic continuum and defect fields, neglecting for simplicity the surface effects.

We represent the deformation and defect concentration as in the above treatment in the form

$$\operatorname{div} \mathbf{U} = \xi,$$

$$n_d = n_{d0} + n_{d1},$$

where ξ_0, n_{d0} are spatially uniform distributions and n_{d1}, ξ_1 are spatially nonuniform variables (assume $\xi_1 \ll \xi_0$, $n_{d1} \ll n_{d0}$). Correspondingly the free energy density

$$F = F_0 + F_1, \tag{4.78}$$

where $F_1 = U_1 - TS_1$, consists of the deformed elastic continuum energy density with allowance for anharmonism

$$U_{1\,\mathrm{elast}} = \frac{K}{2}\xi_1^2 + K\beta_a\xi_1^4, \tag{4.79}$$

(β_a is anharmonism constant) and defect-elastic continuum interaction energy density

$$U_{1\,\mathrm{int}} = -\theta_d n_{d1}\xi_1 - \theta_d n_{d1}\xi_1'. \tag{4.80}$$

Here ξ_1 is a self-consistent part of the deformation due to the nonuniform defect concentration n_{d1}. We take into account also the possible spatially nonuniform deformation due to the external forces ξ_1' (for example, deformation due to initial dislocations).

The entropy density is given by the expression $S = S_0 + S_1$, where

$$S_1 = k(n_{d0} - n_{d1})\ln(V/V_0) + kn_{d1}\ln(V_1/V_0), \tag{4.81}$$

V is the crystal volume, V_1 is the volume of spatially nonuniform phase, V_0 is the volume of space quantation. From Eq. (4.81) we have for the entropy

$$S_1 = -kn_{d1}\ln\delta_1, \tag{4.82}$$

where $\delta_1 = V/V_1$ is the inverse relative volume of the inhomogeneous phase (in the case of periodic DD structure, for example, $\delta_1 = 2$).

Eqs. (4.78 - 4.80) and (4.82) yield the expression for the free energy. It is convenient to express it through the variable n_{d1}. For this aim one can use the equilibrium equation for n_{d1}, which in the considered bulk case is similar to Eq. (4.57), where now $n_d = n_{d0} + n_{d1}$ is the bulk concentration, $\partial n_d / \partial t = 0$, the sign $\|$ is removed and $\tau_d = \infty$ in accordance with the discussion of stationary (equilibrium) state in Sec. 4.3.2. Moreover, one should put $\operatorname{div} \mathbf{U}_f = \xi_1$. Then from Eq. (4.57) one has

$$\xi_1 = \frac{kT}{\theta_d}\frac{n_{d1}}{n_{d0}} \equiv \varepsilon_d X, \tag{4.83}$$

where we introduced the small parameter $\varepsilon_d = kT/\theta_d$; $X = n_{d1}/n_{d0}$ is a dimensionless order parameter of phase transition. Using now Eq. (4.83), we have for the free energy density

$$F_1 = n_{d0}kT\ln\delta_1\left(1 - \frac{\operatorname{sgn} d}{|\varepsilon_d|\ln\delta_1}\xi_1'\right)X + K\varepsilon_d^2\left(1 - \frac{n_{d0}}{n_{dcr}}\right)X^2 + K\beta_a\varepsilon_d^4X^4. \tag{4.84}$$

Here the critical spatially-uniform defect concentration is

$$n_{dcr} = K\frac{kT}{2\theta_d^2}. \tag{4.85}$$

With exceeding of n_{dcr} the phase transition to the state with $n_{d1} \neq 0$ occurs. At $T = \mathrm{const}$ in Eq. (4.84) there are two externally controlled parameters n_{d0} and ξ_1'.

The dependence of the free energy F_1 on the order parameter in the absence of the external local deformation ($\xi_1' = 0$) is shown in Fig. 19 at different values of control parameter n_{d0}. It is seen that at $n_{d0} < n_{dcr}$ the most probable value is $n_{d1} = 0$, which corresponds to the spatially uniform phase. At $n_{d0} > n_{dcr}$ the spatially nonuniform metastable state with $n_{d1} > 0$ is formed. The

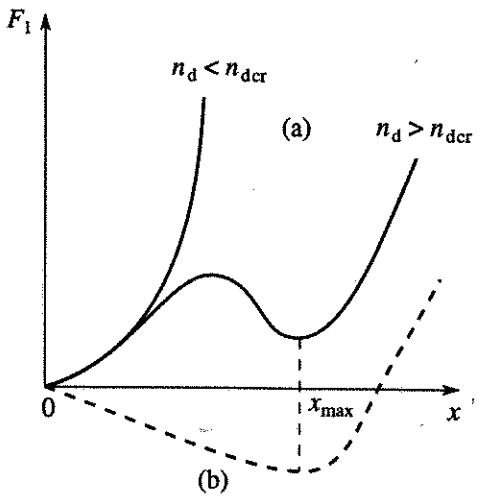

Fig. 19. *Dependence of the free energy F_1 on the defect concentration x of inhomogeneous phase. Formation of metastable state x_m in the absence of external deformation ($\xi_1' = 0$) (a); the case $\xi_1' \neq 0$ (b).*

order parameter depends on the external parameter according to the law ($n_{d0} / n_{dcr} - 1 \ll 1$):

$$n_{d1} \cong \frac{n_{d0}}{|\varepsilon_d|} \left(\frac{n_{d0}}{n_{dcr}} - 1\right)^{1/2},$$

i.e., phase transition of the second kind takes place.

The height of the potential well in which a defect is trapped is

$$W_d \simeq \frac{K}{n_{d1}} \left(\frac{n_{d0}}{n_{dcr}} - 1\right)^2 \simeq 10^2 \left(\frac{n_{d0}}{n_{dcr}} - 1\right) \text{ eV},$$

i.e., W_d is of the order of 1 - 10 eV.

This value may turn out to be larger then the height of the potential barrier of the nonuniform phase formation W_d (see Fig. 19)

$$W_d' \cong \frac{n_{d0}}{n_{d1}} kT \frac{\ln \delta_1}{4}.$$

In this case the stable state is formed.

From Eq. (4.84) one can see that with the help of external local deformation one can eliminate energy barrier of DD structure formation. For this, in the case of vacancies (sgn $d = -1$) the compressive local deformation is needed ($\xi_1' < 0$) and in the case of interstitials (sgn $d = +1$) – the dilatation deformation ($\xi_1' > 0$). The magnitude of the deformation compensating the barrier of inhomogeneous phase formation as follows from Eq. (4.84) is

$$|\xi_1'| = \frac{kT}{|\theta_d|} \ln \delta_1,$$

i.e., $|\xi_1'| \sim 10^{-3} - 10^{-4}$. In Fig. 19b is shown the behavior of the free energy, with allowance for the external deformation, eliminating the barrier. In this case the DD state is stable. From the above consideration it follows that DD structures, (especially localized DD structures) are preferentially formed in the vicinity of initial inhomogeneities of the elastic continuum, for example in the vicinity of dislocations.

4.4. DDI and Subboundary Formation in Laser-Induced Recrystallization of Semiconductor-on-Insulator Films

We now want to show that the theory of DDI in films, developed in Sec. 4.2, with some modifications can be applied for the problem of subboundary formation in laser recrystallization of semiconductor-on-insulator films.

4.4.1. Introduction

The problem of subboundary formation in laser beam recrystallization of amorphous and polycrystalline semiconductor films on insulators used in fabrication of integrated circuits is of great practical and scientific interest (see Refs. [11, 12]). In the process of zone melting recrystallization the molten zone of width l and length L_0 arising due to the action of a laser beam (or some other energy beam) moves along the Si-film of thickness h with scanning velocity $\mathbf{v}$ (see Fig. 20). After the passage of the molten zone the monocrystalline seeds elongated in $\mathbf{v}$-direction and separated by the subboundaries are formed. The subboundaries form quasiperiodic structure with period d in the direction perpendicular to $\mathbf{v}$. Experimental investigations of this effect have revealed the following main facts. The subboundaries consist of the arrays of dislocations elongated parallel to $\mathbf{v}$ [84 - 86] (see Fig. 20). The mean distance between the subboundaries d is proportional to h and for a regime of rather high scanning velocity ($v > 0.1$ mm·s^{-1}) the period d is proportional to $\sqrt{v}$, where $v = |\mathbf{v}|$ [84, 86]. The surface relief of the recrystallized film with the subboundaries is periodically modulated in the direction perpendicular to $\mathbf{v}$ with the period d [85, 93]. The subboundary angular misalignment ψ is inversely proportional to d [87]. The crystallization front in the film is periodically faceted with the subboundaries emerging from the interior corners of the interface (see Fig. 20) [84, 88].

A number of models have been proposed to explain the experimental facts [11, 12]. In our opinion, however, there is no model which from the unified point of view is able to explain all the above-mentioned facts yielding at the same time quantative agreement with experiment, in particular the dependencies $d = d(v, h)$ and $\psi \sim 1 / d$.

In this section we consider a new DD mechanism of subboundary formation in beam induced film recrystallization [89, 90] on the basis of which the quantative theory is developed. The theoretical results obtained are in good agreement with the above experimental results.

The considered DD mechanism consists in the following. We assume that after the solidification of the melt a large number of point defects with concentration n_d are trapped in the film [17, 18]. When defect concentration n_d exceeds a certain critical value n_{dcr} the spatially uniform defect distribution becomes unstable and the formation of one dimensional defect grating begins, with simultaneous appearance of a film bending deformation (Sec. 4.2). Defect clusters then undergo deformationally induced collapse into dislocation loops

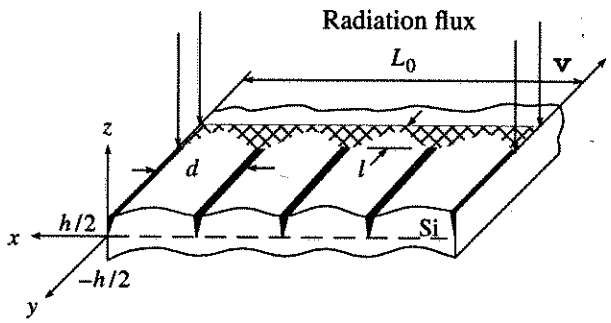

Fig. 20. *Geometry of quasiperiodic subboundaries formation in the model of Si-film with SiO_2 cap at $z > 0$ (see the text).*

(see Secs. 5.1, 5.2), thus forming periodic dislocational pileups, i.e., subboundaries.

4.4.2. Coupled System of Equations for Bending Deformation and Defect Concentration

In practice the multilayered structures are usually used (for example SiO_2–Si–SiO_2). To clarify the basic features of DD mechanism we however use the simplest model of a single Si-film, taking into account the lateral stress $\sigma_{\parallel}$ due to the constrain, imposed by the interface with the SiO_2-film.

Let the z-axis be directed perpendicular to the film, $z = 0$ be in the middle of the film thickness, x-axis be directed perpendicular to vector $\mathbf{v}$ (Fig. 20). In the geometry of Fig. 20 there exist large temperature gradients along the $\mathbf{v}$-direction. The latter give rise to the strong defect fluxes along this direction, hindering the process of periodic defect distribution formation in the $\mathbf{v}$-direction. Due to this the defects grating is formed only along the x-axis. We write an equation for n_d in a one-dimensional approximation, similar to Eq. (4.57)

$$\frac{\partial n_d}{\partial t} = D_d \frac{\partial^2 n_d}{\partial x^2} - \frac{n_d}{\tau_d} - \frac{D_d n_d \theta_d}{kT} \frac{\partial^2}{\partial x^2} \operatorname{div} \mathbf{U}. \qquad (4.86)$$

Under bending deformation we have as usual

$$\operatorname{div} \mathbf{U} = -z\nu \partial^2 \zeta / \partial x^2. \qquad (4.87)$$

In the equation for bending coordinate (4.33) we take into account the lateral stress $\sigma_{\parallel}$ occurring due to the presence of an interface between the Si-film and SiO_2-films:

$$\left.\frac{\partial^2 \zeta}{\partial t^2} + \frac{c^2 h^2}{12} \frac{\partial^4 \zeta}{\partial x^4} - \frac{\sigma_{\parallel}}{\rho} \frac{\partial^2 \zeta}{\partial x^2} - \frac{c^2}{2} \frac{\partial^2 \zeta}{\partial x^2} \left(\frac{\partial \zeta}{\partial x}\right)^2 \right|_{z=0} = \frac{\theta_d}{\rho h} \int_{-h/2}^{h/2} (\nabla n_d)_z \, dz. \qquad (4.88)$$

We note that near the solid-liquid interface only $\sigma_{xx} = \sigma_{\parallel}$ exists while the stress component in the $\mathbf{v}$-direction is negligible, because the solid can freely expand into the melt.

4.4.3. Periodic DD Grating Formation

We suppose that due to the nonuniform distribution of deformation (along the z-axis) in the solid Si-film in SiO_2-Si-SiO_2 sandwich structure, the nonuniform distribution of the defects is established along the z-axis, so that $n_d(h/2) > n_d(-h/2)$ and for simplicity we neglect $n_d(-h/2)$ in comparison with $n_d(h/2)$ in the right-hand side of Eq. (4.88) (see the discussion at the end of this section). We represent the variables in the form $n_d = n_{d0} + n_{d1}$, $\zeta = \zeta_0 + \zeta_1$, $\mathbf{U} = \mathbf{U}_0 + \mathbf{U}_1$ where n_{d0}, ζ_0, $\mathbf{U}_0$ are the solutions spatially uniform along the surface and $n_{d1} = n_{d1}(h/2)$, ζ_1, $\mathbf{U}_1$ are spatially nonuniform perturbations

$$\zeta_1 = \sum_q \zeta_q(t) \exp(iqx) + \text{c.c.},$$
$$n_{d1} = \sum_q n_{dq}(t) \exp(iqx) + \text{c.c.} \qquad (4.89)$$

Then for n_{d1}, ζ_1 we obtain from Eqs. (4.86 - 4.88) the following equations

$$\frac{\partial n_{d1}}{\partial t} = D_d \frac{\partial^2 n_{d1}}{\partial x^2} - \frac{n_{d1}}{\tau_d} + \frac{n_{d0} \theta_d h \nu D_d}{2kT} \frac{\partial^4 \zeta_1}{\partial x^4}, \qquad (4.90)$$

$$\frac{\partial^2 \zeta_1}{\partial t^2} + \frac{c^2 h^2}{12} \frac{\partial^4 \zeta_1}{\partial x^4} - \frac{\sigma_{\parallel}}{\rho} \frac{\partial^2 \zeta}{\partial x^2} - \frac{c^2}{2} \frac{\partial^2 \zeta_1}{\partial x^2} \left(\frac{\partial \zeta_1}{\partial x}\right)^2 = \frac{\theta_d n_{d1}}{\rho h}. \qquad (4.91)$$

We put $\sigma_{\parallel} = -\theta n_{d0}$ assuming that the stress due to the presence of defects (vacancies) exceeds the thermal and Si–SiO_2 lattice mismatch stresses. Eqs. (4.90) and (4.91) are the closed system of equations describing the spontaneous formation of DD (bending) structures in the film.

4.4.4. Linear Regime of Instability

Putting in Eq. (4.89) $\zeta_q(t) = \zeta_q \exp(\lambda t)$, $n_{dq}(t) = n_{dq} \exp(\lambda t)$ and neglecting the nonlinear term in Eq. (4.91) we obtain under the condition $\lambda^2 \ll q^4 c^2 h^2 / 12$ for the growth rate λ:

$$\lambda = \lambda(q) = (R_d l_0^2 q^2 / (1 + l_0 q^2) - D_d q^2 - \tau_d^{-1}), \qquad (4.92)$$

where the control parameter R_d and l_0 are as follows

$$R_d = 6\theta_d^2 \nu n_{d0} D_d / \rho c^2 kT h^2,$$
$$l_0^2 = \rho c^2 h^2 / 12 \sigma_{\parallel}.$$

As it follows from Eq. (4.92) the dependency $\lambda = \lambda(q)$ can have a maximum $\lambda = \lambda_{max}$ when $q = q_{max}$

$$\lambda_{max} = [R_d^{1/2} - (D_d / l_0^2)^{1/2}]^2 - 1/\tau_d,$$
$$q_{max} = \frac{1}{l_0} [(R_d l_0^2 / D_d)^{1/2} - 1]^{1/2}. \qquad (4.93)$$

From Eq. (4.93) one can see that $\lambda_{max} > 0$ if

$$R_d > R_{dcr} = \left[(D_d / l_0^2)^{1/2} + \tau_d^{-1/2}\right]^2 \qquad (4.94)$$

and q_{max} is real if $R_d > D_d^2 / l_0$. Thus if $R_d > R_{dcr}$ (i.e., the critical vacancy concentration is exceeded) the Fourier amplitudes of the coupled grating of bending deformation and defect concentration begin to grow exponentially in time. The Fourier harmonic with $q = q_{max}$ has the maximum growth rate $\lambda = \lambda_{max}$ and is dominant in the excitation spectrum. In the following we confine ourselves to consideration of the grating with $\lambda = \lambda_{max}$ and $q = q_{max}$.

4.4.5. Nonlinear Stationary Regime

The stabilization of the instability occurs due to the nonlinearity of bending deformation. In stationary regime ($\partial n_d / \partial t = 0$, $\partial^2 \zeta_1 / \partial t^2 = 0$) from Eqs. (4.90), (4.91), and (4.89) where $\zeta_q(t) = \zeta_q = \text{const}$, $n_{dq}(t) = n_{dq} = \text{const}$ and $q = q_{max}$ we obtain the expression for the stationary Fourier amplitude of the film bending deformation static wave

$$\zeta_q = \frac{h}{\sqrt{6}} \left[\frac{R_d}{D_d q^2 + 1/\tau_d} - 1 - \frac{1}{l_0^2 q^2} \right]^{1/2}. \quad (4.95)$$

As one can see from the comparison of Eqs. (4.92) and (4.95) the real value of ζ_q appears under the fulfillment of the critical condition (4.94). For the amplitude of the defect concentration wave one has

$$n_{dq} = R_d \rho c^2 h^3 q^4 \zeta_q / 12\theta_d (D_d q^2 + \tau_d^{-1}). \quad (4.96)$$

Close to instability threshold

$$(\sqrt{R_{dcr}} < \sqrt{R} < \sqrt{R_{dcr}} + 2/\sqrt{\tau_d})$$

under the condition $|\theta_d| / kT \gg 1$ from Eqs. (4.89) and (4.96) ($q = q_{max}$) one obtains for the deformation

$$\zeta_1 = \frac{2h}{\sqrt{3}} \frac{(R_{dcr}\tau_d^{-1})^{1/4}}{(D_d q^2 + \tau_d^{-1})^{1/2}}$$

$$\times [(R_d/R_{dcr})^{1/2} - 1]^{1/2} \cos q_{max} x. \quad (4.97)$$

The formation of bending deformation grating (4.97) occurs as a phase transition when the concentration of defects exceeds the critical value n_{dcr} following from Eq. (4.94) ($|\theta_d| / kT \gg 1$):

$$n_d > n_{dcr} = \rho c^2 kTh^2 / 6\theta_d^2 \nu D_d \tau_d. \quad (4.98)$$

Well above the threshold when $R_d \gg R_{dcr}(n_{d0} \gg n_{dcr})$ and $D_d q_{max}^2 \gg 1/\tau_d$ from Eqs. (4.95) and (4.89) we find for the deformation

$$\zeta_1 = \frac{2h}{\sqrt{6}} (|\theta_d| / 2kT)^{1/4} \cos q_{max} x. \quad (4.99)$$

Similarly from Eqs. (4.96), (4.99), and (4.89) for the concentration grating one has

$$n_1 = \text{sgn} d\, 4\sqrt{6} n_{d0}^2 a^3 (|\theta_d| \nu / 2kT)^{7/4} \cos q_{max} x. \quad (4.100)$$

As is seen from Eqs. (4.99) and (4.93) the period of DD grating is

$$\Lambda_d = 2\pi / q_d$$

$$= 2\pi h (12 a^3 n_{d0})^{-1/2} [(|\theta_d| / 2kT)^{1/2} - 1]^{-1/2}. \quad (4.101)$$

Thus the periodic coupled static DD wave is formed in the film due to the DD instability with defects being self-trapped in potential wells.

4.4.6. Periodic Subboundary Formation. Comparison of Theoretical and Experimental Results

In Sec. 5 it is shown that the defect clusters are unstable with respect to transition to the localized state with formation of dislocation loops (Sec. 5.2). If these processes of spontaneous generation of dislocations take place in spatially periodic defect clusters formed due to DD instability described by Eq. (4.100), then as a result the periodic arrays of dislocations (i.e., subboundaries) are formed with period given by Eq. (4.101).

Thus we have obtained the periodic subboundaries with the same period as the undulation of the surface (Fig. 20). This picture corresponds to the experimental data [85]. As follows from Eq. (4.100) the subboundaries (which correspond to maxima of $n_{d1}(x)$) are located in the case of vacancies in the valley of the surface relief (min $\zeta_1(x)$) (Fig. 20), i.e., in the compressed regions. It is known that in the compressed Si the melting temperature is decreased (see Sec. 5.3.2 and Ref. [81]). Due to this the crystallization front on the surface of the film must be faceted with interior corner locations coinciding with the locations of subboundaries (Fig. 20), which in fact is experimentally observed [91].

Let us discuss the formula for the period of subboundaries (4.101) in the case of vacancy mechanism. To estimate n_{v0} we note that in the experimental conditions the melt duration at a given point is equal to $\tau = l / v$ (we assume that local melting and solidification occur instantly with the onset and the end of illumination). During this time interval τ the concentration of generated vacancies reaches the value $n_{v0} = g_v \tau = g_v l / v$, where $g_v = g_v(T)$ is vacancy generation rate in the melt (see the discussion at the end of the section). Taking the above-obtained expression for n_{v0} into account we obtain from Eq. (4.101):

$$\Lambda_v = \text{const}\, (v)^{1/2} h, \quad (4.102)$$

where

$$\text{const} = \frac{2\pi}{\sqrt{12}} (g_v a^3 l)^{-1/2} [(|\theta_d| \nu / 2kT)^{1/2} - 1]^{-1/2}$$

and for the values of v under consideration $\partial T / \partial v = 0$ [92].

Thus the DD mechanism explains two basic experimental dependencies of the distance between the subboundaries $\Lambda_{v\,exp} \sim h$ and $\Lambda_{v\,exp} \sim \sqrt{v}$ [84, 86]. Now we show that Eq. (4.102) yields also quantative agreement with experimental results [84, 86]. According to Eq. (4.102) for $h = 5 \times 10^{-5}$ cm we obtain the dependency $\Lambda_v = 3 \times 10^{-3} \sqrt{v}$, where $[v] = \text{mm} \cdot \text{s}^{-1}$ [84]. For $T \sim 1.4 \times 10^3$ K, $\theta_v = Ka^3 \sim 10^{-11}$ Erg ($K \sim 5 \times 10^{11}$ Erg·cm^{-3}, $n^{-1} = a^3 \sim 2 \times 10^{-23}$ cm^3), using $v = v_{exp} = 0.1$ mm·s^{-1}, $l = l_{exp} = 1$ mm in Eq. (4.102) we estimate the vacancy generation rate as $g_v = 2 \times 10^{19}$ cm^{-3}·s^{-1}. At these values of parameters the estimated value of $n_{v0} \sim 2 \times 10^{20}$ cm^{-3} and $n / n_{v0} = 2.5 \times 10^2 = n v / g_v l$, and experimental dependency [84] is well reproduced. According to Eq. (4.98)

$$n_{vcr} = (kT/|\theta_v|)(1/6va^3)(D_v/D_z),$$

if $\tau = h^2/D_z$, where D_z is the coefficient of diffusion along the z-axis. For $D_v/D_z \sim 10$ we have $n_{vcr} \sim 10^{20}$ cm^{-3} and the critical condition (4.98) is fulfilled. One can see from Eq. (4.99) that

$$\psi = 2\partial\zeta/\partial x|_{x=\pi/2} = \text{const}\, q_{max} \sim 1/\Lambda_d.$$

Such dependency was found experimentally in Ref. [87].

The important question pertaining to the DD mechanism of subboundary formation considered here is: what is the nature of vacancy generation in Si melt with the assumed generation rate $g_v = g_v(T)$?

We propose here the following mechanism of vacancy generation in the SiO_2–Si–SiO_2 structure.

It is known that very intensive dissolution of oxygen from the SiO_2 interface into the Si melt occurs during the melt duration. In the process of Si melt solidification, oxygen atoms move back to interface forming SiO_2, leaving a vacancy in the film. Thus, the situation is similar to the pump of vacancies in laser-induced oxidizing of Si surface in air (see Ref. [16] and Sec. 4).

Assume that the concentration of vacancies trapped in the solidified melt is proportional to the concentration of oxygen atoms dissolved during the melt duration l/v. Then the generation rate $g_v = g_v(T)$ is in fact the dissolution rate of oxygen during the melt duration. The deep dips in the concentration distribution of oxygen trapped in solidified Si film at the SiO_2–Si interface [93] seem to corroborate this hypothesis. From this point of view the nature of the interface in SOI structures is of primary importance for the problem of subboundary formation in zone melting recrystallization.

Another important aspect of influence of interfaces is connected with the symmetry of the SOI structure. We considered asymmetrical binary structure SiO_2–Si, and assuming the interface defect generation mechanism, postulated asymmetry of vacancy distribution along the z-axis.

As a result we obtained a bending DD grating with period d proportional to the thickness of the film h. In the sandwich SOI structure SiO_2–Si–SiO_2 or in multilayer structure the symmetry of vacancy distribution along the z-axis can also be violated due to asymmetry of thermal conductivity conditions at two opposite interfaces of the Si-film with the SiO_2. In this case the bending DDI still takes place with the period of DD grating proportional to the film thickness. But in those cases where the symmetry of vacancy concentration is restored, bending deformation is impossible and is replaced by the longitudinal deformation of the film with symmetrical undulations of the opposite surfaces of the Si-film, the period of which (and thus that of subboundaries) is independent of the film thickness. The experimental data of Ref. [93] correspond to this picture.

Thus the DD mechanism of subboundary formation in beam recrystallization of Si-on-insulator film, developed in this section (see also Refs. [89, 90]) is able under reasonable assumptions to explain basic experimental results. From the viewpoint of DD mechanism the subboundaries are formed as a result of DD instability and phase transition of the second kind under exceeding of the critical concentration of point defects (vacancies) trapped in the Si-film during rapid solidification of the melt. Further theoretical studies of this problem, in particular the development of the theory of DD instability with longitudinal deformation of the film, are urgently required.

5. THRESHOLD EXTENDED DEFECT FORMATION IN SOLIDS

In Secs. 3 and 4 we studied formation of the periodic point defect structures on the surfaces and in films. Now we want to show that the same DD mechanisms which are effective in formation of periodic defect-deformational structures in systems with boundaries lead to the formation of localized DD structures in the bulk, i.e., extended defects: voids and dislocation loops.

It is well known that under the action of external energy fluxes a large number of voids and dislocation loops are formed in solids. Thus, intense generation of voids takes place after ion implantation [21, 94 - 96], irradiation with high energy particles [20] and laser irradiation [97]. A common feature of all these cases is the generation of a large number of nonequilibrium vacancies. The cause of the void formation is condensation of these defects into clusters which are embryonic voids. The classical theory of the voids generation has a very limited applicability in the above-mentioned cases due to the very high vacancy concentrations and nonequilibrium conditions of their generation. Moreover, the sharp threshold character of the void formation observed in experiments [98, 99] cannot be explained from the classical (thermodynamic) point of view.

In Secs. 5.1 and 5.2 vacancy-strain (VS) mechanism of the nonequilibrium threshold formation of voids and dislocation loops in solids is considered. The physical essence of it consists in the following. The external action (irradiation, injection, implantation, etc.) creates large densities of nonequilibrium vacancies in solids. A fluctuational increase of the vacancy field causes a local nonuniform compression of the medium. Due to this, in accordance with the model of rigid inclusions [30, 31], there appears a force acting on the elastic continuum. This force causes the appearance of the vacancy flux, directed into the compressed region, which leads to the positive feedback and VS instability development when a certain critical value of the vacancy concentration n_v is exceeded. The instability is stabilized by the nonlinearity of the elastic continuum. As a result, vacancies accumulate in the compressed region created by themselves, in this way forming a vacancy cluster. Due to the deformational energy barriers (see Sec. 5.2) the diffusion of vacancies out of the cluster is strongly suppressed. The threshold vacancy concentration predicted by the proposed theory ($n_{vcr} \cong 10^{19}$ cm^{-3}) is in agreement with the experimental values obtained in the

investigation of threshold void formation during ion implantation [99].

In Sec. 5.1 we consider the mechanism of cluster formation, using the ad hoc assumption about the character of medium nonlinearity, taking into account only the cubic strain term. This simplification enables one to develop a Landau-type theory of cluster formation as a phase transition of the second kind and obtain an analytical expression for the number of vacancies condensing into a cluster. In Sec. 5.2 we use the empirical law for the dependence of pressure in solids on strain, taking into account an infinite series of powers of the medium strain. The effective nonlinear diffusion equation governing the process of cluster formation is thus derived and is solved analytically, yielding expressions describing the shape of the cluster and the strain inside it. The same mechanisms as those considered in Secs. 5.1 and 5.2 can be used also for the description of other point defect (interstitial or doping atom) clustering.

The cluster of point defects is unstable with respect to formation of voids or dislocation loops. Depending on the number of vacancies in the cluster it may assume either a spherical (in isotropic medium approximation) shape (void) or a disk shape of monolayer thickness, i.e., a dislocation loop. In Sec. 5.2 we study the conditions of either voids or dislocation loop formation from the point defect clusters depending on temperature and the size of clusters.

It is usually accepted that the main cause of dislocation generation in crystals under the action of laser light is shear stress generation due to nonuniform heating, similar to generation due to mechanical stress [100]. In accordance with this point of view, dislocations cannot be generated in the case of uniform laser irradiation. The strain-induced mechanism of laser-induced generation of dislocations due to spontaneous condensation of nonequilibrium vacancies (or interstitials), pumped by laser radiation, considered here is not connected with the presence of laser-induced shear stresses and must take place also in the case of uniform illumination. The theory developed here on the basis of VS mechanism enables one to estimate the radius of generated dislocation loops, their number density and the threshold value of vacancy concentration (Sec. 5.1).

In Sec. 5.3.1 we apply the concept of threshold extended defect formation for developing the theory of degradation of injection lasers. It is shown in Sec. 5.3.2 that this concept enables one also to draw an interpretation of the experimentally observed effect of anisotropic melting of semiconductor surfaces under the action of laser radiation with pulse duration $\tau_p = 1\ \mu s$ - 1 s (see also Sec. 4.3.2). In Sec. 6 the mechanism of cumulative explosive damage of semiconductors by a train of subthreshold laser pulses is developed on the basis of the mechanism of threshold condensation of the point defects' field.

5.1. Threshold Laser Pumping of Point Defect Clusters [101, 102]

The equation for the vacancy concentration n is as follows:

$$\frac{\partial n_v}{\partial t} = D_v \Delta n_v - \frac{1}{\tau_v} n_v + G_v - \frac{D_v \theta_v}{kT} \operatorname{div} (n_v \operatorname{grad} \xi), \tag{5.1}$$

G_v is the rate of vacancy generation by an external source. The equation for the deformation is given by ($\xi = \operatorname{div} \mathbf{U}$):

$$\frac{\partial^2 \xi}{\partial t^2} = c_l^2 \Delta \xi + c_l^2 \beta_a \Delta \xi^3 - \theta_v \rho^{-1} \Delta n_v, \tag{5.2}$$

where β_a is the elastic continuum anharmonicity constant, $\theta_v = -Ka^3$. Contrary to Secs. 2 and 4, we do not impose here any boundary conditions on n_d and the vector $\mathbf{U}$.

The closed system of Eqs. (5.1) and (5.2) has the stationary spatially uniform solution

$$n_{v0} = G_v \tau_v, \quad \xi_0 = \operatorname{div} \mathbf{U}_0 = 0.$$

First, let us investigate the stability of this solution. ξ and n_v are represented in the form

$$n_v = n_{v0} + n_{v1}, \quad |n_{v1}| \ll n_{v0},$$

$$n_{v1} = N^{-1} \sum_q N_q \exp (i\mathbf{qr} + \lambda t), \tag{5.3}$$

$$\xi_1 = N^{-1} \sum_q \xi_q \exp (i\mathbf{qr} + \lambda t), \tag{5.4}$$

where N is the number of atoms in a crystal.

Substituting Eqs. (5.3) and (5.4) into Eqs. (5.1) and (5.2) and neglecting nonlinear terms with respect to perturbations, we obtain the following expression for the growth rate at the threshold of instability

$$\lambda = -D_v (1 - n_{v0} \theta_v^2 / \rho c_l^2 kT) q^2 - \tau_d^{-1}. \tag{5.5}$$

If the vacancy concentration exceeds the critical value:

$$n_{v0} > n_{vcr} = \rho c_l^2 kT / \theta_v^2, \tag{5.5a}$$

i.e., if $G_v > G_{cr} = \rho c_l^2 kT / \tau_v \theta_v^2$, the effective diffusion coefficient becomes negative, and any fluctuation of the vacancy density field grows and becomes more sharp. For $T \simeq 10^3$ K, $n_{vcr} \simeq 10^{-3}$, $a^{-3} \sim 10^{19}$ cm^{-3}.

Stabilization of the VS-instability takes place due to the elastic continuum anharmonicity. In a steady state, neglecting vacancy sink and putting $\tau^{-1} = 0$ (for justification of this assumption see below) from Eqs. (5.1) and (5.2) we obtain:

$$n_{v1} = -n_{v0} (\theta_v / kT) \xi_1, \tag{5.6}$$

$$\Delta \left[\left(1 - \frac{n_{v0}}{n_{vcr}}\right) \xi_1 + \beta_a \xi_1^3 \right] = 0. \tag{5.7}$$

In the approximation of independent modes, substituting Eq. (5.4), where $\lambda = 0$, into Eq. (5.7) we have

$$(n_{v0}/n_{vcr} - 1)\,\xi_q = \beta_a \xi_q |\xi_q|^2. \tag{5.8}$$

Now, one can express ξ_1 in terms of ξ_q

$$\xi_1 = N^{-1}\sum_q \xi_q \exp(i\mathbf{qr}) = (V/8\pi^3 N) \times \int \xi_q \exp(i\mathbf{qr})\, d\mathbf{q}, \tag{5.9}$$

where V is the volume of the crystal.

Substituting the expression for ξ_q derived from Eq. (5.8) in Eq. (5.9), we obtain:

$$\xi_1 = -\frac{1}{n\beta_a^{1/2}}\left(\frac{n_{v0}}{n_{vcr}} - 1\right)^{1/2} \delta(\mathbf{r}), \tag{5.10}$$

where $n \equiv a^{-3}$.

According to Eq. (5.6), the inhomogeneous vacancy field is connected with the strain field:

$$n_{v1} = \frac{n_{v0}|\theta_v|}{nkT\beta_a^{1/2}}\left(\frac{n_{v0}}{n_{vcr}} - 1\right)^{1/2} \delta(\mathbf{r}). \tag{5.11}$$

Thus, we obtained the δ-like distribution, which corresponds to formation of the vacancy cluster. As one can see from Eqs. (5.10) and (5.11) the process of cluster formation occurs as a phase transition of the second kind with the spatially homogeneous vacancy concentration n_{v0} being the control parameter and inhomogeneous concentration n_{v1} being the order parameter.

A vacancy cluster formed as a result of the VS-instability can assume a spherical shape or collapse to a disk of monolayer thickness, i.e., form a void or dislocation loop. To show this, one should use the approach enabling one to obtain the shape and finite size of a vacancy cluster. Such an approach is developed in the next section.

5.2. Strain and Shape of Metastable Point Defect Cluster. Formation of Voids and Dislocation Loops [102]

Let us consider in more detail the vacancy clustering effect and the resulting formation of voids and dislocation loops. The vacancy field is described by the diffusion equation with the strain-induced vacancy drift. In approximation of an isotropic medium we have:

$$\partial n_v/\partial t = \nabla\left[D_v \nabla n_v - (D_v/kT)\, n_v \mathbf{F}\right], \tag{5.12}$$

where $\mathbf{F}_v = -\nabla(\partial U / \partial n_v)$ is a force acting upon one vacancy, U is the elastic energy of a unit volume of the medium with vacancies:

$$U = -\int_0^{\xi} P\, d\xi = -\int_0^{\xi} \{\exp[-\beta(\xi + \Omega n_v)] - 1\}\,\alpha^{-1} d\xi \tag{5.13}$$

Here P is the pressure, $\Omega \equiv a^3$. Due to the high pressures in the core of a vacancy cluster it is necessary to take into account nonlinear dependence of pressure on compression. Here we use the following empirical dependence [103]:

$$p(\xi) = \alpha^{-1}(\exp(-\beta\xi) - 1), \tag{5.14}$$

where α and β are determined by relations $\beta / \alpha = K$, $1 + \beta = -K'$, where K' is the bulk modules pressure derivative at zero pressure [103]. When compression is small this equation transforms into the ordinary equation of the linear theory of elasticity. Moreover, in Eq. (5.13) we take into account that the vacancy induced strain is

$$\xi_v = -\Omega n_v. \tag{5.15}$$

From Eqs. (5.12) and (5.13) we obtain the following nonlinear equation for vacancy concentration

$$\partial n_v/\partial t = \nabla[D_v \nabla n_v - (D_v/kT)\, n_v \nabla\{(\Omega/\alpha) \times \exp(-\beta(\xi + \Omega n_v))\,(1 - \exp(\beta\xi))\}]. \tag{5.16}$$

In the same way, we obtain an equation for the medium strain:

$$\rho \partial^2 \xi/\partial t^2 = -\nabla^2[(1/\alpha)\exp(-\beta(\xi + \Omega n_v))]. \tag{5.17}$$

We introduce here the assumption of bulk modules dependence on vacancy concentration:

$$K = K_0\left(1 - \frac{n_v}{n}\right), \tag{5.18}$$

n is the number of atoms per unit volume. The dependence (5.18) is the simplest analytic model of lattice softening at large vacancy concentrations due to which the strain collapse stabilization occurs.

Further on we can use Eq. (5.17) in the adiabatic approximation, putting $\partial^2\xi / \partial t^2 = 0$, because the time of static strain field formation is far less then the characteristic diffusion time. In this case, substituting Eq. (5.17) into Eq. (5.16), after simple transformations we obtain the closed equation for dimensionless concentration of vacancies

$$\partial u/\partial\tau = \nabla[D(u)\nabla u],$$
$$u = n_v/n_{cr},\ \tau = tD_v n_{cr}^{2/3},\ \nabla = (\partial/\partial\eta, \partial/\partial\chi, \partial/\partial\kappa), \tag{5.19}$$

where $\eta = xn_{cr}^{1/3}$, $\chi = yn_{cr}^{1/3}$, $\kappa = zn_{cr}^{1/3}$ are coordinates, and the critical vacancy concentration $n_{cr} = kT / K\Omega^2$ coincides, by the order of magnitude, with Eq. (5.5a), because $K = \rho c_1^2 - 4\mu / 3$.

The dimensionless diffusion coefficient $D(u) = 1 - [u(1 - \varepsilon u)]\exp(-\beta\varepsilon u)$.

Eq. (5.19) is the nonlinear diffusion equation with the coefficient $D(u)$ depending on vacancy concentration. This dependence is shown in Fig. 21. When vacancy concentration exceeds the value $n_{1cr} \simeq n_{cr}$ the diffusivity becomes negative, and any vacancy density

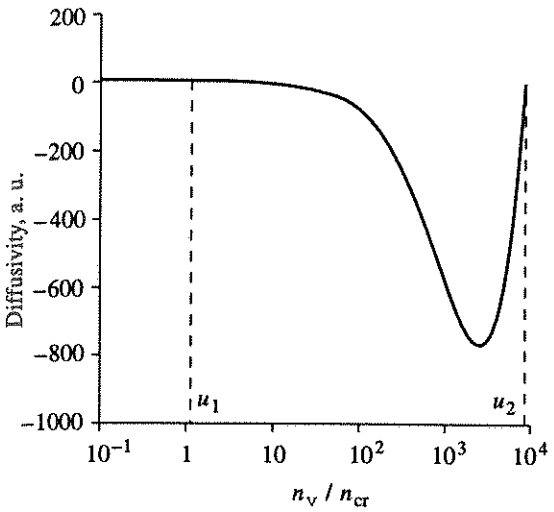

Fig. 21. *Effective diffusion coefficient of a vacancy D in dependence on the vacancy concentration $u = n_v / n_{cr}$ (in accordance with Eq. (5.19), $\beta = 10$, $\varepsilon = 10^{-4}$, $D(u_1) = D(u_2) = 0$, $u_1 = 1.001$, $u_2 = 6776$.*

fluctuation begins to become sharper in space. Thus, as the critical concentration is exceeded, the vacancy field collapses into clusters whose shape and size may be determined from the static solution of Eq. (5.19). Static solution of Eq. (5.19) is obtained from the following nonlinear equation:

$$\Delta u = -[d\ln|D(u)|/du](\nabla u)^2. \qquad (5.20)$$

Here we restrict ourselves to consideration of the one-dimensional case, which corresponds to the strongly anisotropic medium where a particular direction (for example, x) exists, along which the diffusion preferentially occurs. In this case in Eq. (5.20)

$$\nabla = \frac{\partial}{\partial\eta}, \Delta = \frac{\partial^2}{\partial^2\eta^2},$$

and it may be solved analytically. In order to do this, introduce a new variable $v \equiv du/d\eta$. Then, eliminating η in Eq. (5.20), we obtain:

$$dv/v = -[d\ln|D(u)|/du]\,du. \qquad (5.21)$$

The variables are separated and the solution has the form:

$$v = C/D(u),$$

where C is an arbitrary constant. We shall obtain the solution of the one-dimensional Eq. (5.20) from this equation, using the above-introduced definition of v:

$$\eta = C\int D(u)\,du + C_1. \qquad (5.22)$$

The constants in this expression may be determined from the physical conditions: C_1 is the shift along the coordinate axis (space position of the whole cluster), and C determines the number of vacancies in a cluster and should be chosen so that a cluster size obtained from Eq. (5.22) corresponds to the real void sizes. For instance, for voids with size 200 Å observed in Ref. [104] $C \sim 10^{-6}$. In a general case the size of a void will be determined by the number of vacancies in local fluctuation, and therefore the average radius of originating voids is determined by the probability of such fluctuation. It will require further investigation to determine exactly the size of the originating voids, depending on driving conditions.

The vacancy concentration dependence on the coordinate, given by Eq. (5.22) is shown in Fig. 22. It has a peak in the middle and extremely steep edges. Based on these results, one can expect that in the three-dimensional case a vacancy cluster formed in such a way would have a core with extremely large vacancy concentration and sharp boundaries. As one can see from Eq. (5.15), a static localized compressive strain is coupled with the cluster, shown in Fig. 23. Thus, vacancies are trapped inside the self-consistent strain well.

Due to the high point defect concentration in the region of a cluster it may serve as a seed for a void or a dislocation loop. In the idealized one-dimensional case considered above we obtained a vacancy cluster in the form of a plane layer. In a real anisotropic medium (crystal) one should expect the formation of crystallographically faceted or disk-shaped vacancy clusters. These clusters are unstable under certain conditions with respect to collapse into voids or disks of monoatomic thickness (i.e., the dislocation loops [105]), leading to minimization of their free surface. Consequently, either voids or dislocation loops are formed, depending on relative values of energies of their formation. Dislocation loops are formed under the following condition [17]:

$$\frac{1}{3}\mu\frac{1}{1-\sigma}br^2[\ln(r/a)+Z]+\pi r^2\gamma' - 2\pi(r/a)\alpha_0 kT < 4\pi\left(\frac{3}{4}r^2a\right)^{2/3}\gamma_{cl}, \qquad (5.23)$$

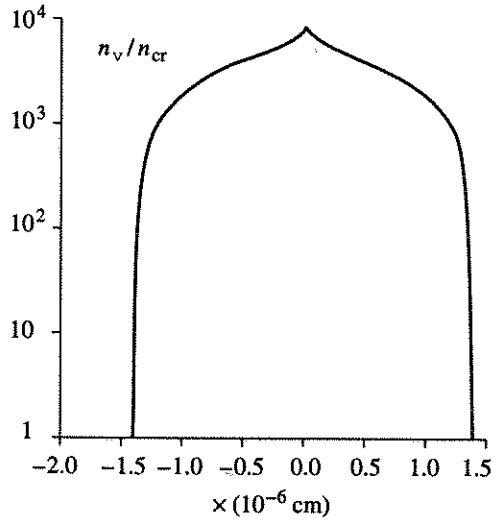

Fig. 22. *Shape of vacancy cluster $u = u(x)$ in the one-dimensional case in accordance with the formula (following from Eq. (5.22)): $\eta = \pm\{u - u_2 + (1/\beta\varepsilon)\exp(-\beta\varepsilon u_2)[(1-2/\beta)\times\{(\exp(-\beta\varepsilon(u-u_2))-1)(u+1/\beta\varepsilon)+u-u_2\}]-\varepsilon\{(\exp(-\beta\varepsilon\times(u-u_2))-1)u^2+u^2-u_2^2)\}\}$, where $x = C\eta n_{cr}^{-1/3}$, $C = 1.5\times10^{-6}$, $\beta = 10$, $\varepsilon = 10^{-4}$.*

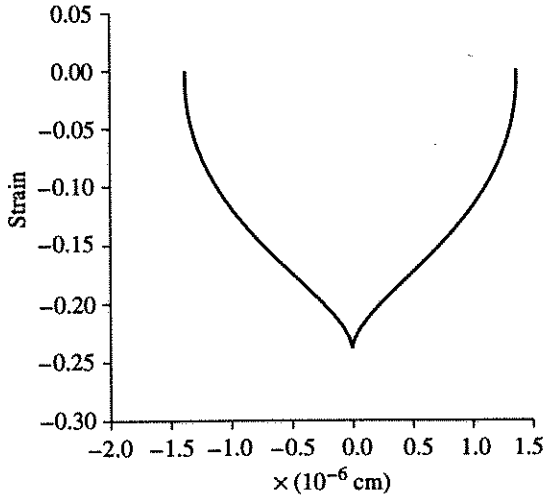

Fig. 23. *Deformation well, coupled with vacancy cluster (in accordance with Eq. (5.15)). The values of parameters are the same as in Fig. 22.*

where b is a Burgess vector, equal in this particular case to the interatomic distance a, r is the loop radius, σ is the Poisson ratio, μ is the shear modulus, γ' is the energy of the stacking fault created by the loop, $z \approx 2$ is a constant, which takes into account the strain energy in the core of the dislocation, $\alpha_0 \approx 3$ is the coefficient which takes into account a change of the entropy of a crystal per atom in the dislocation core, and γ_{cl} is the specific surface free energy of the cluster.

The expression in the left-hand side of Eq. (5.23) is the free energy of the dislocation loop formed from the vacancy disk of monoatomic thickness. In the right-hand side of Eq. (5.23) there appears the surface energy of a spherical cluster, which has the same volume as the disk-shaped cluster.

Taking $\gamma' = 10 - 10^2$ erg·cm^{-2}, $\gamma_{cl} = 10^2 - 10^3$ erg·cm^{-2}, $\mu = 10^{11}$ erg·cm^{-3}, $b = 5 \times 10^{-8}$ cm, $T = 10^3$ K, we obtain that Eq. (5.23) is fulfilled (i.e., dislocations are formed) if the dislocation loop radius is $r < 10a \sim 5 \times 10^{-7}$ cm (see Fig. 24).

The theory developed in Sec. 5.1 enables one to estimate the radius of the generated dislocation loops. The number of vacancies accumulated in the cluster, according to Eq. (5.11) is equal to

$$N_v = \int n_{v1} dr = \frac{n_{v0}|\theta_v|}{nkT\beta_a^{1/2}} \left(\frac{n_{v0}}{n_{vcr}} - 1\right)^{1/2}. \quad (5.24)$$

If these vacancies form a disk of monoatomic thickness (dislocation loop) its radius is

$$r_{dis} = a\left(\frac{N_v}{\pi}\right)^{1/2} = a\left[\frac{n_{v0}|\theta_v|}{\pi nkT}\right]^{1/2} \frac{1}{\beta_a^{1/4}} \left(\frac{n_{v0}}{n_{vcr}} - 1\right)^{1/4}. \quad (5.25)$$

In a wide region of values of β_a and n_{v0}, for the dislocation loop radius we have $r_{dis} \sim 10a \sim 5 \times 10^{-7}$ cm.

Thus, the mechanism considered here predicts vacancy condensation into clusters when the threshold concentration n_{vcr} is exceeded, and formation, mainly, of dislocation loops, the number density of which can be estimated as $n_{v0} / N_v \sim 10^{17}$ cm^{-3}.

Apart from laser irradiation, a dense vacancy field can be formed by other types of radiation. For instance, irradiation with high-energy particles (with ion, electron or neutron beams) must lead to generation of a large number of point defects, which can condense into clusters and eventually form the dislocation loops. Note in this connection that in Ref. [106] the formation of a dense net of small dislocation loops with an average loop radius of about 3 nm was observed in neutron irradiated copper species. It is in good agreement with the estimates of dislocation loop sizes obtained in Sec. 5.1. Additionally, the model of dislocation formation under the influence of external radiation presented here predicts preferential generation of dislocations in the deformed regions of the medium, for instance, near the initial dislocations (see the general discussion of the DD structure formation in Sec. 4.3.4). This in fact was observed in Refs. [105, 106].

Note that the mechanism of defect cluster formation considered here is similar to the polaron formation in ion crystals with the autolocalization of the electron in the deformed region of the crystal lattice, created by the same electron [137].

According to the mechanism considered here, powerful laser radiation (along with other types of radiation) can pump a dense field of dislocations in a solid. Small dislocation loops under sufficiently long ($>10^{-3}$ s) irradiation grow due to trapping of point defects. In its turn, the large density dislocation field is unstable: when a certain critical density of dislocations is exceeded a dislocation-strain instability (similar to VD-instability described here) develops which leads to the periodic dislocation structure formation.

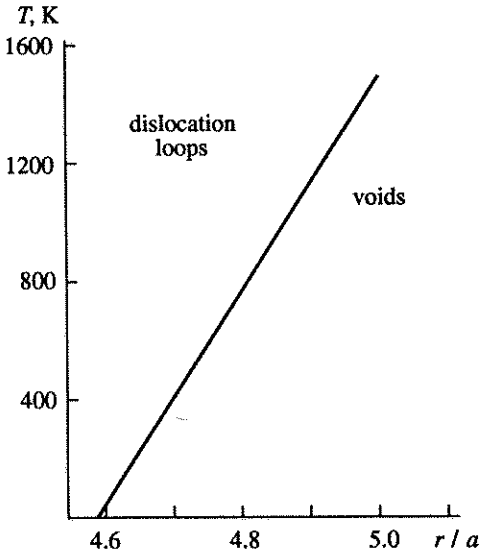

Fig. 24. *Diagram of void dislocation loops creation in accordance with Eq. (5.23).*

Two types of periodic dislocation structures were observed experimentally: interplane structures (in the form of ideally straight lines, reflecting the crystal symmetry of the surface (see Sec. 7.2) and in-plane structures (or vein structures) (see Sec. 7.1).

The models of strain-diffusion instabilities describing dislocation self-organization by climbing and gliding were developed to explain the formation of these two qualitatively different types of dislocation structures (see Secs. 7.1 and 7.2).

The above mechanism of vacancy cluster formation may be responsible for the phenomena of degradation of optoelectronics devices (Sec. 5.3.1) and anisotropic melting of semiconductors by laser irradiation (Secs. 5.3.2 and 4.3.1).

The effect considered is valid also for other types of point defects and dopants that are described by the model of rigid inclusions. For example, it may describe the interstitial clustering, leading to the dislocation loop formation, and clustering of impurities. The duration of these processes t may be estimated as $t \sim d^2 / D_{dif}$. Here d^2 is the distance between separated clusters and D_{dif} is the effective diffusivity. Taking into account a strong strain-induced increase of the effective diffusivity modules (see Fig. 21) we obtain for the above-described case of vacancies that $t \sim 10^{-5}$ s. We believe here that the vacancy diffusion coefficient is about 10^{-9} cm^2·s^{-1} at equilibrium vacancy concentration.

From the point of view of free energy of the DD structures (Sec. 4.3.5), a point defect cluster is a local metastable self-consistent state of coupled point defects and strain fields.

5.3. Applications of the Concept of Diffusional-Deformational Threshold Condensation of Point Defects

5.3.1. Mechanism of Threshold Degradation of Optoelectronic and Light Emitting Devices

Degradation phenomena in optoelectronic devices are of great importance from the practical point of view [2, 108]. In this section we want to show that the effect of threshold formation of the DD structures (clusters, voids, and dislocation loops), together with the mechanism of recombination-stimulated point defect generation can explain the experimental results obtained in studies of degradation phenomena. We do so with an example of degradation of injection lasers.

Investigation of operation of the heterolasers has revealed two most typical stages of their degradation: initial gradual degradation, logarithmically depending on time, and after a certain moment, rapid ("catastrophic") degradation. The following empirical equation is established experimentally for the injection laser lifetime τ (the gradual degradation stage duration [109]):

$$\tau = \Lambda_0^{-1} \exp\left(E_a/kT - \gamma I_0\right), \qquad (5.26)$$

where γ, Λ_0, E_a are the empirical constants, T is the temperature, I_0 is the driving current. The physical mechanism leading to such behavior, and in particular to Eq. (5.26) has not yet been clarified.

In this section the microscopic mechanism of the semiconductor lasers' degradation is proposed. Based on it, the existence of two the above-mentioned degradation stages is explained, and in addition a derivation of Eq. (5.26) is performed. Good agreement with the experimental data is obtained.

The physical essence of the mechanism being proposed consists in the following [102]. Creation of nonequilibrium electron-hole pairs by the external action (in this case, by an injection) leads to the recombination-enhanced point defect generation (see for example Ref. [110] and Sec. 3). Gradual accumulation of point defects during the laser operation corresponds to the gradual degradation stage. When concentration of point defects exceeds a critical value n_{vcr} the threshold generation of extended defects (dislocations) begins (Secs. 5.1 and 5.2).

It is this intense threshold dislocation generation due to the above-described vacancy-strain (VS) (or interstitial-strain) mechanism that leads to the rapid degradation of a laser diode (at the rapid degradation stage a dense dislocation net formation was observed experimentally [111]).

Let us proceed to the derivation of Eq. (5.26) for gradual stage duration τ, which in accordance with the above-described VS-mechanism, is equal to the time interval in which the point defect concentration n_v reaches the critical value n_{vcr}, i.e.,

$$n_{vcr} = G_v \tau . \qquad (5.27)$$

We use the following explicit expression, derived in the theory of recombination-enhanced defect creation [110] for defect generation rate G_v in Eq. (5.27):

$$G_v = 4(\pi)^{1/2} \left(N_e N_a V_0 / \hbar (kT)^{3/2}\right) \left(d d_a / \varepsilon_0 r_{av}^3\right)^2 \times (E_f - \varepsilon_{ex})^{1/2} \exp\left[-(E_f - \varepsilon_{ex})/kT\right], \qquad (5.28)$$

where N_{ex}, N_a are the densities of excitons created by injection, and of atoms in a crystal, respectively; V_0 is the mean volume of interaction between a lattice atom and an exciton; d, d_a are the dipole moment of an exciton and of an atom, respectively; ε_0 is the dielectric permeability of the medium; r_{av} is the average radius of the interaction between an atom and an exciton; E_f is the energy of a point defect formation; and ε_{ex} is the exciton energy. Exciton energy in the case of electron injection into the conduction band may be estimated as $\varepsilon_{ex} = E_g + eV$, where e is the electron charge, V is the electric potential on the p-n junction, E_g is the band gap.

From Eqs. (5.27) and (5.28) we obtain the microscopic expression for τ:

$$\tau = n_{vcr}/G_v = \Lambda_0^{-1} \exp\left[(E_f - \varepsilon_{ex})/kT\right], \qquad (5.29)$$

where

$$\Lambda_0 = (K\Omega_v^2/kT)\,4\,(\pi)^{1/2}\,(N_{ex}N_a V_0/\hbar\,(kT)^{3/2}) \times (dd_a/\varepsilon_0 r_{av}^3)^2\,(E_f-\varepsilon_{ex})^{1/2}. \quad (5.30)$$

If we assume that the operating point lies on an approximately linear part of the current-voltage characteristic (CVC) of a laser diode, then $V = I_0 / s$, where s is the CVC steepness. Then Eq. (5.29) may be expressed exactly in the form of Eq. (5.26):

$$\tau = \Lambda_0^{-1}\exp\,(E_a/kT - \gamma I_0)\,, \quad (5.31)$$

where

$$\gamma = e/skT, \quad (5.32)$$

$$E_a = E_f - E_g. \quad (5.33)$$

Let us show now that the values of microscopic expressions in Eqs. (5.31 - 5.33) are in agreement with empirical values in Eq. (5.26) obtained in Ref. [109].

When $s \sim 2 \times 10^2$ mA·V^{-1}, $T \sim 10^2$ K from Eq. (5.32) we have $\gamma \sim 10^{-1}$ mA^{-1}, and when $K \sim 10^{12}$ erg·cm^{-3}, $N_a \sim 10^{23}$ cm^{-3}, $N_{ex} \sim 10^{18}$ cm^{-3}, $V_0 \sim 10^{-18}$ cm^3 [110], $\varepsilon_0 \sim 10$, $r_{av}^3 \sim 10^{-18}$ cm^3, $d \sim 10^{-18}$ esu, $d_a \sim 10^{-19}$ esu [110], $E_a \sim 1$ eV, from Eq. (5.30) we obtain $\Lambda_0 \sim 10^6$ h^{-1}. These numerical estimates of γ, Λ_0, E_a are close to the empirical values [109].

Thus, the microscopic degradation mechanism of laser diodes which consists in recombination-enhanced point defect (for instance, vacancy and interstitial) generation and their spontaneous condensation into dislocation loops under exceeding of the critical defect concentration n_{dcr} yields the microscopic expression for gradual degradation stage duration τ which is in good qualitative and quantitative agreement with the empirical formula. A similar expression is obtained in the case of excitation of electron-hole pairs instead of excitons.

5.3.2. Nonuniform Light-Induced Melting of Semiconductor Surface

One of the possible manifestations of deformation-induced condensation of defects in clusters and threshold formation of extended defects, considered in Secs. 5.1 and 5.2, is the effect of anisotropic melting of the semiconductor surface under the action of light [112 - 114, 138]. This effect consists in appearance of local melted regions on the surface of Si [114] or Ge [138] under the action of optical radiation (CO_2 and Nd : YAG lasers [138], Xe lamps [114]). The form of these regions (triangles, squares) depends on the crystallographic symmetry of the surface, while their dimensions and number density depend on the pulse duration and light intensity [114]. This effect takes place under both uniform and nonuniform illumination, so that it cannot be related to the generation of dislocations due to the shear stresses. It has threshold character and occurs as the threshold energy density $10 - 10^2$ J·cm^{-2} is exceeded. Moreover, the number density of the locally melted regions increases with the initial defectivity of the crystal (for example, after ion implantation).

From the viewpoint of the DDI theory of defect clustering, exposed in Secs. 5.1 and 5.2, the mechanism of the effect of nonuniform melting can be developed along the same lines as the theory of the threshold degradation of optoelectronic devices (Sec. 5.3.1).

Laser radiation generates the field of point defect concentration in the subsurface layer of a semiconductor with the generation rate depending on intensity and wavelength of the radiation. After a certain irradiation time, when concentration of point defects reaches the threshold value, the process of defect clustering begins, according to the DD-mechanism. Due to high compressive strain inside the vacancy cluster (see Fig. 23) the melting temperature inside the cluster on the Si surface is lowered (by approximately 100 K at $P \sim 10$ kbar [81]). Accordingly, the cluster regions are melted prior to the melting of other regions. Thus, the melting threshold time (at a given radiation intensity) is equal to the time of reaching the critical point defect concentration.

Note that the condensation of light-generated point defects occurs preferentially near the initial inhomogeneities of the crystal dopants, initial dislocations and other defects, which enhances either the point defect generation rate (Sec. 3.1), or the probability of defect cluster formation (Sec. 4.3.5), or favorably influences both these processes. This fact explains the experimental fact of increase of the density of locally melted regions with the increase of the initial defectivity of the surface (for example due to ion implantation). In the case of periodic point defect surface structure formation the nonuniform melting of the surface occurs accordingly periodically (see Sec. 4.3.1).

We can estimate the generation rate necessary for reaching the threshold concentration $n_{vcr} \sim 10^{19}$ cm^{-3}·s^{-1} using $n_{vcr} = G_v\tau$ and the experimental value of the threshold irradiation time τ (at I = const). For Xe-lamp $\tau \sim 1$ s and $G_v \approx 10^{19}$ cm^{-3}·s^{-1}, for Nd : YAG laser $\tau \sim 3 \times 10^{-3}$ s and $G_v \sim 10^{21}$ cm^{-3}·s^{-1}.

5.3.3. Cumulative Explosive Damage of Semiconductors by Train of Subthreshold Laser Pulses

We proceed now to consideration of multishot laser damage effect from the viewpoint of the concept of threshold condensation of point defects.

Multishot laser damage (MLD) of optical components is a very important problem in laser technology. The MLD effect is a universal phenomenon, observed in metals, semiconductors and transparent dielectrics. Understanding of the nature of small accumulative structural changes, leading to sudden catastrophic damage induced by multiple irradiation of material by relatively weak ultrashort laser pulses is the prerequisite for successfully solving this problem. At present vast experimental data have been obtained regarding MLD in different materials.

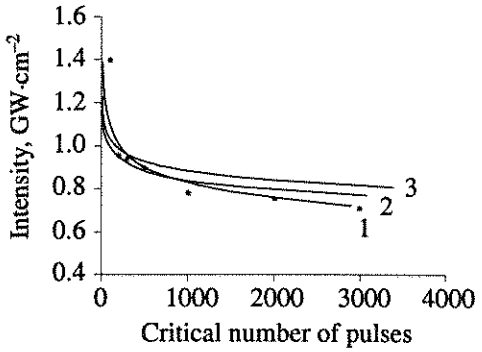

Fig. 25. *Dependence of critical number of laser pulses leading to damage on the intensity of a pulse in series: the points are experimental data for Si from Ref. [119]; solid curves are calculated according to Eqs. (5.46) and (5.49) with E_d = 0.8 eV (1), E_d = 0.85 eV (2), E_d = 0.9 eV (3). Values of other parameters in Eqs. (5.46) and (5.49) are given in the text.*

The cumulative effect in metals was investigated in many works [3]. In Ref. [115] MLD was investigated in Cu and Ag mirrors. The typical result of the experiment is the increase of the threshold number of pulses m_{th} leading to damage with decreasing intensity of each pulse (Fig. 25).

However, accumulation of microscopic structural changes prior to the macroscopic damage was not clarified. The diagnostic methods exploited in Refs. [116 - 118] were sensitive only to the macrodamage and were not helpful in determining the nature of the accumulation process.

The MLD effect in semiconductors was investigated in Ref. [119], where it was shown that in Si the dependence of threshold number of pulses on pulse intensity $m_{th} = m_{th}(I)$ is similar to that in metals, and there exists the minimum intensity I_{th} below which no damage occurs at any number of pulses (Fig. 25).

The MLD effect was investigated also in transparent isolators, in alkali halides and plastics (see Ref. [120]). In general, the obtained results concerning the dependence $m_{th}(I)$ and I_{th} correspond to those found for opaque media. For the explanation of the MLD-effect two principally different mechanisms were proposed. The statistical mechanism (SM) of Ref. [121] assumes that there exists the finite probability of damage by a single pulse at any intensity. There is experimental evidence both in favor of SM mechanism [121] and against it [122]. It seems likely that the SM mechanism describes only the damage due to the initial defectiveness of the crystal.

Another approach is based on the idea of certain gradual microscopic structural changes, being accumulated from pulse to pulse (see Ref. [120]). It was assumed in Ref. [123] that a gradual pileup of dislocations occurs under MLD in metals with formation of periodical dislocation structures leading to increase of absorption and eventual damage.

In the recent model of Ref. [124] it was assumed that under MLD the point defects, generated due to localization of energy of excited electron-hole pairs on some atoms in a crystal lattice, are accumulated from pulse to pulse. The point defect accumulation induces local stresses, leading, as the threshold stress value is exceeded, to plastic deformation, which, in the author's opinion, is the beginning of rapid and irreversible changes of optical properties of the material. This model corresponds well to the experimental results on MLD in alkali halides.

In this section we use the idea of point defect accumulation for developing the model of MLD in strongly absorbing semiconductors [125]. As in Sec. 3, we assume the thermal fluctuation mechanism of point defect generation with energy of defect formation decreasing due to laser-induced local electronic excitation, heating, deformation and due to the defect-induced deformation. The last aspect is of primary importance for the mechanism of MLD developed here because it leads to explosive defect accumulation, similar to some extent to the thermal explosion in the exothermal chemical reaction or explosive crystallization (see Sec. 8). The principal difference between the thermal explosion and the point defect concentration explosion lies in the nature of the positive feedback in these processes: in the first case it is effected through the temperature field and in the latter ones – through the deformation (strain) field.

The model of MLD developed here, with no or only slight modifications can be applied also to dielectrics and metals.

We focus here mainly on the problem of multishot damage in semiconductors (we have taken Si as an example), illuminated by a series of short ($\tau \sim 10^{-10}$ s) laser pulses with the wavelength in the absorbing region of the spectrum (λ = 532 nm, $\gamma = 10^4$ cm^{-1}, the repetition rate Δt^{-1}, r_0 is laser spot radius, $r_0\gamma \gg 1$).

The essence of the proposed mechanism of the cumulative damage in strongly absorbing semiconductors is as follows. Due to laser pulse-produced heating, laser-induced strain and decrease of formation energy the enhanced formation of point defects occurs in a thin ($h_d \approx 10^{-5}$ cm) subsurface layer (Sec. 3). The rate of defect production is greater than the recombination rate because the equilibrium concentration, corresponding to the renormalized formation energy and elevated temperature, is much higher than that prior to laser pulse action. Between the laser pulses the medium cools down practically to its initial temperature, because the time interval between the pulses Δt is larger than the effective time of temperature relaxation.

At the same time, laser-generated point defects (vacancies and interstitials) do not have enough time to disappear from the defect-enriched layer of thickness h_d during the time interval between successive pulses. The defects bring about lattice strain resulting in a decrease of their own formation energy. This leads to more efficient defect generation during the next pulse.

When the concentration of point defects n_d reaches the critical value n_{dcr} of extended defect formation the spatially uniform distribution of generated defects becomes unstable and formation of defect clusters and voids begins (Secs. 5.1 and 5.2). We assume here that with further increase of point defect concentration at higher threshold concentration

$$n_{damage} = \beta_d n_{dcr}, \quad (5.34)$$

where $\beta_d \gg 1$, the fusion of voids into the cracks occurs, which signifies the beginning of damage. Note that the cracks, i.e., void pileups, can be formed as a periodic structure (see Sec. 6). Thus, Eq. (5.34) is the postulated damage criterion, which we shall use in the following consideration.

The main assumption of the MLD model under consideration is that the field of point defect concentration in a crystal is unstable intrinsically. This means that accumulation of a certain type of point defects decreases the formation energy of these defects, which corresponds to the attraction between them.

As a model of collective defect interaction we take an elastic interaction described by Eq. (1.1). The medium strain consists of two parts

$$\operatorname{div} \mathbf{U} = \operatorname{div} \mathbf{U}_d + \operatorname{div} \mathbf{U}_L,$$

where $\operatorname{div} \mathbf{U}_d$ is the strain due to defects and $\operatorname{div} \mathbf{U}_L$ is strain due to laser-induced heating and plasma excitation. Strain of the medium $\xi_d = \operatorname{div} \mathbf{U}_d$ due to the presence of concentration of point defects n_d is found from Eq. (5.2). In the stationary case we obtain, using $K \equiv \rho c_l^2$, $\beta_a = 0$, $v \to d$

$$(\operatorname{div} \mathbf{U})_d \equiv \xi_d = \Omega_d n_d; \ \Omega_d = a^3 \operatorname{sgn} d. \quad (5.35)$$

It follows from Eqs. (5.34) and (5.35) that $H_d = -\theta_d \Omega_d n_d$ and the defect formation energy F_d is given by

$$F_d = E_d - \theta_d \Omega_d n_d. \quad (5.36)$$

Here

$$E_d = E_{d0} - E_{ee} - \theta_d \operatorname{div} \mathbf{U}_L, \quad (5.37)$$

where E_{d0} is the thermal-fluctuation formation energy, E_{ee} is the energy of local electronic excitation, decreasing the effective formation energy (Sec. 3).

The rate of temporal change of the relative concentration of defects $N_d = n_d / n$ is determined by competition of the generation rate G_d, recombination rate R_d and diffusion

$$\partial N_d / \partial t = D_d \partial^2 N_d / \partial x^2 + G_d - R_d, \quad (5.38)$$

where D_d is the diffusion coefficient. Eq. (5.38) assumes different forms during the pulse and in the time interval between the pulses.

During the pulse due to the high value of equilibrium concentration

$$N_d^{eq} = \exp\left[-(E_d - |\theta_d| N_d^{eq}) / kT\right],$$

where the temperature $T = T(I)$ is a function of laser intensity. Due to the low diffusion on the time scale of pulse duration, one can neglect recombination and diffusion in Eq. (5.38). Thus, during the pulse the rate of change of relative defect concentration can be obtained from Eq. (5.38), where G_d is given by the expression for the thermal fluctuating defect generation rate, with allowance for Eq. (5.36)

$$\partial N_d / \partial t = G_d = \nu_D \exp\left[-(E_d - |\theta_d| N_d) / kT\right], \quad (5.39)$$

where ν_D is the Debay frequency. To find concentration of defects, generated during the pulse, we assume that T in Eq. (5.39) is equal to its value averaged over the pulse duration. Then, from Eq. (5.39) we obtain the additional number of defects generated by one mth pulse

$$\Delta N_m^+ = \varepsilon_d \ln\left[1 - \nu_D \tau_p \varepsilon_d^{-1} \times \exp\left[-(E_d - |\theta_d| N_d(-\tau_p)) / kT_p\right]\right], \quad (5.40)$$

where $N_d(-\tau_p)$ is the relative defect concentration after the action of $(m-1)$th pulse, $\varepsilon_d = kT_p / |\theta_d|$.

After the end of the pulse the temperature falls to room temperature during the time $\gamma^{-2}\chi^{-1} = 10^{-7}$ s $\ll \Delta t$ ($\chi = 0.1$ cm^2·s^{-1}, $\Delta t = 10^{-2}$ s), the electronic excitation and laser-induced strain in Eq. (5.37) disappear in a time interval of the order of carrier recombination time $\tau \ll \Delta t$ (for Si $\tau = 10^{-7}$ s). Thus, after the end of the pulse the generation rate (5.39) sharply falls and is insignificant during the time interval between the pulses, i.e., during the time interval Δt one can put $G_d = 0$ in Eq. (5.38).

Thus, at the time interval between the pulses the diffusion and recombination of defects are the only important processes and are described by equations

$$\partial N_d / \partial t = D_d \partial^2 N_d / \partial z^2 - N_d / \tau_d, \quad \partial N_d / \partial z|_{z=0} = 0, \quad (N_d)_{t=0} = N_d(0) h_d \delta(z), \quad (5.41)$$

where $\tau_d = l_d^2 / D_d$ is the defect lifetime (l_d is the mean distance between the defects sinks), $N_d(0)$ is the defect concentration on the surface at a time moment $t = 0$, which corresponds to the end of the mth pulse.

The solution of this problem is as follows

$$N(z, t) = h_d / (2\pi D_d t)^{1/2} \int_0^\infty \{\exp[(-(z-\xi)^2 / 4D_d t)] + \exp[(-(z+\xi)^2 / 4D_d t)]\} (N_d)_{t=0} d\xi,$$

whence for defect concentration on the surface one obtains

$$N_d(z = 0, t) = N_d(0) h_d (\pi D_d t)^{-1/2} \exp[-t/\tau_d].$$

Hence, the number of defects which recombine or diffuse away at a time interval Δt between two successive pulses and no longer participate in cooperative interaction is given by

$$\Delta N_m^- = N_d(0) (1 - h_d (\pi D_d \Delta t)^{-1/2} \exp[-\Delta t / \tau_d]). \quad (5.42)$$

The inequality $\Delta N_m^+ - \Delta N_m^- > 0$ yields the criterion of the beginning of defect accumulation: the number of

defects generated during the pulse must be higher than the number of annihilated ones in the time between the two sequential pulses Δt. From the critical condition $\Delta N_m^+ = \Delta N_m^-$, we obtain the equation for the threshold temperature T_{th} after the exceeding of which the defect accumulation begins

$$\nu_D \tau_p \exp\left[-E_d/kT_{th}\right] = \left[\exp\left(-E_d/kT_0\right) + \Delta N_d^+\right](1-C), \tag{5.43}$$

where $C = h_d (\pi D_d \Delta t)^{1/2} \exp\left[-\Delta t/\tau_d\right]$.

We rewrite Eq. (5.43) in the form

$$T_{th} = E_d/k \left(\frac{E_d}{kT_0} + \ln \nu_D \tau_p C\right). \tag{5.44}$$

Thus, the threshold temperature is approximately proportional to the defect formation energy. Because $T = T(I_L)$, Eq. (5.44) determines the threshold value of intensity I_{th} below which no damage occurs after action of any number of pulses.

At $T > T_{th}$ one can neglect recombination and diffusion of defects between the pulses due to the exponential dependence of G_d – Eq. (5.39) – on temperature. Then, integrating Eq. (5.39) we obtain the defect concentration after the end of the mth pulse

$$N_m = -\varepsilon_d \ln\left[1 - mA/\varepsilon_d\right],$$

where $A = \nu_D \tau_p \exp\left[-E_d/kT_p\right]$.

Equating N_m to the relative concentration of defects at which damage occurs (5.34) we obtain the equation for determining the number of pulses leading to damage

$$1 - mA/\varepsilon_d = \exp\left[-\beta_d N_{cr}/\varepsilon_d\right]. \tag{5.45}$$

Using Eq. (5.5a) for N_{cr} we have $\beta_d N_{cr} / \varepsilon_d = \beta_d \rho c_l^2 / K \approx \beta_d \gg 1$. Substituting $\exp(-\beta_d) \approx 0$ in Eq. (5.45) we obtain the following equation for the critical number of pulses m:

$$m_{cr} = (kT_p/|\theta_d|)\,(1/\nu_D \tau_p) \exp\left[E_d/kT_p\right]. \tag{5.46}$$

Now, we have to find the dependence $T = T(I)$. For the absorption coefficient we use the following formula [119]

$$\gamma(T) = \gamma_0 \exp\left[T/T_s\right], \tag{5.47}$$

where γ_0 and T_s are constant. Due to $\tau_p \gg \tau_{e\text{-}ph} \sim 10^{-12}$ s, where $\tau_{e\text{-}ph}$ is the electron-phonon relaxation time, we can use the heat conduction equation. Because the heat diffusion length $l = (\chi \tau_p)^{1/2} \approx 10^{-6}$ cm, we can neglect heat diffusion and write

$$\partial T/\partial t = I(1-R)\,\gamma_0 \exp\left[T/T_s\right]/c_v. \tag{5.48}$$

From Eq. (5.48) we obtain the temperature at the end of the pulse

$$T_p = T_0 - T_s \ln\left[1 - I(1-R)\,\gamma_0 \tau_p e^{\frac{T_0}{T_s}}/(T_s c_v)\right] \tag{5.49}$$

Eq. (5.49) determines the temperature T in Eq. (5.46).

Using Eqs. (5.46) and (5.49), we carried out computer calculations of the critical number of laser pulses m_{cr}, after which the damage occurs. We used the values of parameters corresponding to experimental conditions of Ref. [119]: $\tau_p = 80$ ps, $\Delta t = 0.01$ s, $R = 0.37$ (at 532 nm), $c_v = 0.678$ J·cm^{-3}, $\gamma_0 = 5 \times 10^3$ cm^{-1}, $T_s = 430°$ K, $\nu_D = 10^{13}$ s^{-1}, $\theta_d = Ka^3 = 10^{-10}$ erg ($K = 10^{12}$, $a^3 = 10^{-22}$ cm^{-3}). The only free parameter is the defect formation energy E_d, which was varied in a vicinity of 1 eV.

The calculated dependence of the critical number of pulses on pulse intensity is shown in Fig. 25, in comparison with the experimental results of Ref. [119]. It is seen that the present mechanism of accumulative explosive laser damage can well reproduce the experimental dependence. The shape of the curve $m_{cr} = m_{cr}(I)$ shown in Fig. 25 is typical also for other materials [120].

In conclusion, the mechanism of accumulative laser damage is developed. In accordance with this mechanism the laser pulse generated defects give rise to the appearance of the medium strain which decreases the defect formation energy, thus creating the positive feedback. As a result, the dynamics of defect accumulation from pulse to pulse is similar to thermal explosion. Two successive threshold processes determine the microscopic picture of the accumulative damage.

The first one is the threshold formation of clusters of point defects and voids, and the second one is the threshold fusion of voids into cracks leading to damage.

6. FORMATION OF PERIODIC RING VOID STRUCTURES IN LASER VAPOR DEPOSITION OF METAL FILMS

In Sec. 5 we studied the formation of extended defects due to DDI of point defects. When the concentration of extended defects, generated due to the strain-induced condensation or due to any other mechanism, exceeds certain critical values the field of extended defect interacting with elastic continuum may become unstable and the DDI of extended defects develops, leading to the formation of extended defect periodic structures. We proceed now to the consideration of these instabilities. In Sec. 6 we consider the void DDI and in Sec. 7 – two types of the dislocation DDI.

6.1. Theory of Void Diffusional-Deformational Instability

One of the processes accompanied by intensive void formation is laser-induced deposition of metal films. It is known that many excess vacancies are formed inside the deposited layer during condensation at sufficiently low temperatures ($T < T_m/3$, where T_m is the melting temperature) [19]. The number of excess vacancies is reduced, in particular, through their condensation into stable complexes of macrovoids (Secs. 5.1, 5.2). The cylindrical through-macrovoids are formed in this way in thin films with thickness $h \sim 100$ nm [19]. This process is accompanied by the formation of additional

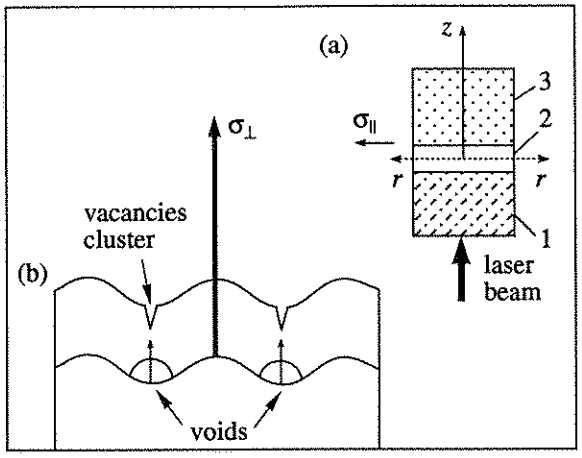

Fig. 26. *Film on the glass substrate. 1 – substrate, 2 – film, 3 – carbonyl. $\sigma_{\parallel}$ is lateral stress in the film due to laser heating of the sandwich film-substrate system (a). Part of the film on the glass substrate in the deformed state. Due to the instability the voids form periodic pileups at the interface, locally decreasing $\sigma_{\perp}$. The vacancies in the upper half of the film are automatically accumulated in the compressed regions, forming narrow clusters (channels) (b).*

interfaces between gaseous phase, metallic film, and substrate, but thermodynamically this state turns out to be more favorable than the system of randomly distributed vacancies [19].

The accepted opinion is that the voids are randomly distributed throughout the film. In this section we want to show that an ensemble of voids can make a transition into a spatially ordered state, forming the periodic rings (concentric ring macrovoids), when the number of voids exceeds a certain critical value [127].

The periodic macrovoid structures are formed as a result of the development of a void DDI, consisting in the following. A thin film, which is coupled to the substrate, can be subjected to the fluctuations of the bending deformations. Such an initial bending deformation is accompanied by the occurrence of spatially periodic areas of dilation and contraction of the film. These deformations lead to development of the directed vacancy fluxes, which give rise to the directed void fluxes. Spatially periodic piles of voids are formed at the interface due to resultant deformation-induced transfer of voids, giving rise to a periodic stress modulation, perpendicular to the plane of the film. The substrate thus produces a periodic force, which acts on the film, thereby amplifying the initial deformations and leading to the onset of instability. We consider a thin film with the thickness h, having interfaces with the substrate 1 and vacuum 3 (Fig. 26a). The z-axis is directed from the surface $z = 0$ into vacuum (Fig. 26b) and r is the radius vector in the xy-plane (Fig. 26b).

The temperature gradient along the z-axis and the difference of thermal expansion coefficients of the film and the substrate as well as the lateral bell-shaped temperature distribution lead to the occurrence of externally applied stresses in the film: along the z-axis ($\sigma_{\perp}$), and a lateral stress $\sigma_{\parallel}$ (Fig. 26a).

We write the equation for the bending coordinate ζ (see Sec. 4.3) in the form

$$h\rho\frac{\partial^2\xi}{\partial t^2} + \frac{h^3c^2}{12}\rho\Delta_r^2\xi - h\sigma_{\parallel}\Delta_r\xi + f_{NL}(\xi) = \sigma_{\perp}(1 - S_0N), \tag{6.1}$$

where f_{NL} accounts for the nonlinearity of bending deformations (cf. Eq. (4.33)). The right-hand side of Eq. (6.1) takes into account the local decrease of $\sigma_{\perp}$ in the film due to the formation at a given point r of the cylindrical voids with number density N [cm^{-2}] and cross-sectional area (Fig. 26b) (the cylinder axis is along the z-axis).

We assume that these voids with the number density $N(r)$ are formed by vacancy condensation either via the strain-induced mechanism of Sec. 5.2, or some other mechanism. Because the remaining gas of vacancies is adjusted adiabatically to the ensemble of voids we can put

$$N = \beta n_v,$$

where $\beta = \text{const}$, n_v is the bulk density of vacancies.

As was shown in Secs. 1 and 4 the deformation occurring in the film gives rise to a deformation-induced drift of vacancies. Now we want to demonstrate that the diffusion and drift of vacancies lead to diffusion and drift of voids.

We denote the strain in the film

$$\xi = \text{div } \mathbf{U} = -z\Delta_r\zeta \tag{6.2}$$

and represent the variables ξ, N, n_v, and ξ in the form

$$\zeta = \zeta_0 + \zeta_1, \quad N = N_0 + N_1$$
$$n_v = n_{v0} + n_{v1}, \quad \xi = \xi_0 + \xi_1,$$

where $\zeta_0 = 0$, N_0, n_{v0}, and ξ_0 are the mean, spatially uniform values and ξ_1, N_1, n_{v1}, and ξ_1 are the fluctuations.

The vacancy flux is determined by the equation

$$\mathbf{j}_{v1} = -D_v \text{grad } n_{v1} - \frac{D_v|\theta|n_{v0}}{kT}\text{grad div } \mathbf{U}_1, \tag{6.3}$$
$$|\theta| = Ka^3 \equiv |\theta_v|.$$

Due to the presence of the vacancy flux, the velocity of the void movement is equal to

$$\mathbf{V}_{void} = -a^3\mathbf{j}_{v1}. \tag{6.4}$$

The void flux is then $\mathbf{j}_{void} = N_0\mathbf{V}_{void}$. Taking this formula as well as Eqs. (6.3) and (6.4) into account, we obtain the diffusional and drift terms in the continuity equation for the fluctuation of a number density of voids

$$\frac{\partial N_1}{\partial t} = D\Delta_r N_1 - \frac{D|\theta|N_0}{kT}\Delta_r \text{div } \mathbf{U}_1, \tag{6.5}$$

where $D = a^3n_{v0}D_v$ is the coefficient of the resultant void diffusion due to the adsorption and emission of

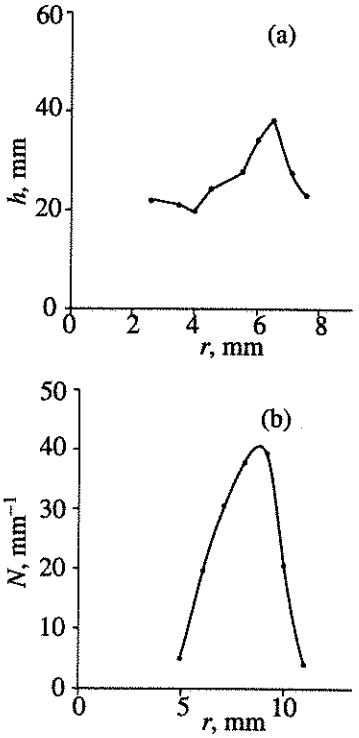

Fig. 27. *Dependence of metal film thickness at an intermediate stage of deposition (a); the radial density distribution of ring voids N(r) (b).*

vacancies. In deriving the diffusional term in Eq. (6.5) we used $N = \beta n_v$.

Now we express div $\mathbf{U}_1$ in Eq. (6.5) through ζ_1. It will be shown below that the void ordering takes place only in the lower half of the film, where $z < 0$ (here the fluctuations grow in time). In the upper half ($z > 0$) the fluctuations are damped out. With the aim of describing the movement of the lower halves of the voids, let us put in Eq. (6.2) $z = -h/4$. We have div $\mathbf{U}_1 = h/4\Delta\zeta_1$. Taking this relation into account, we represent Eq. (6.5) in the form

$$\frac{\partial N_1}{\partial t} = D\Delta_r N_1 - g\Delta_r^2\zeta_1, \tag{6.6}$$

where

$$g = \frac{hDN_0|\theta|}{4kT}. \tag{6.7}$$

Linearizing Eq. (6.1), we have

$$\frac{\partial^2\xi_1}{\partial t^2} - c_\parallel^2\Delta_r\xi_1 + \frac{c^2h^2}{12}\Delta_r^2\xi_1 = -RN_1, \tag{6.8}$$

where we denote

$$c_\parallel^2 = \frac{\sigma_\parallel}{\rho}, \quad R = \frac{\sigma_\perp S_0}{h\rho}.$$

Eqs. (6.6) and (6.8) constitute a closed system of equations describing void DDI in a linear nonstationary regime, to which we shall confine our consideration in this section. To find the stationary solution one must evidently take into account the term f_{NL} in Eq. (6.1) (cf. Sec. 4.2).

Seeking the solution of the system (6.6), (6.8), we assume that the dependence on r, which is determined by the temperature distribution, is slow in comparison with the characteristic scale of the structure (this assumption is valid for the experimental situation, discussed below, where the characteristic scale of the structure observed is $d \simeq 3 \times 10^{-3}$ cm, Fig. 27b). Thus we may put $c_\parallel = \text{const}$ and seek the solution of the system (6.6), (6.8) in the form

$$N_1(r,t) = (AJ_0(qr)\,e^{\lambda t},\ \xi_1(r,t)) = AJ_0(qr)\,e^{\lambda t}, \tag{6.9}$$

where A and B are constants, $J_0(qr)$ is a Bessel function of the first kind. In accordance with Eq. (6.9) the fields of void concentration and bending deformation form concentric ring structures (Fig. 2) with their center at $r = 0$, and whose amplitudes grow in time with the growth rate λ. From Eqs. (6.6), (6.8), and (6.9) we obtain the system of two-linear homogeneous algebraic equations for A and B. The condition that the determinant of this system vanishes leads to the dispersion equation determining the dependence $\lambda = \lambda(q)$:

$$(\lambda + Dq^2)\,(\lambda^2 + q^2c_\parallel^2 + \frac{c^2h^2}{12}q^4) = Rgq^4. \tag{6.10}$$

For $q^2c_\parallel^2 \gg \lambda^2$ (this condition is in fact satisfied in experiments of Ref. [127]) we have from Eq. (6.10)

$$\lambda = -Dq^2 + \frac{bq^2}{1 + l_0^2q^2}, \tag{6.11}$$

where

$$b = \frac{Rg}{c_\parallel^2}, \quad l_0^2 = \frac{c^2h^2}{c_\parallel^2 12}.$$

The void DDI arises for $\lambda > 0$. In the upper half of the film ($z > 0$), as it can be seen from Eq. (6.6), one has $g < 0$. Thus, according to Eq. (6.11), instability is absent in the upper half of the film.

The dependence $\lambda = \lambda(q)$ according to Eq. (6.11) for $b > D$ is shown in Fig. 28. The maximum value $\lambda = \lambda_{max}$ is reached at the point $q = q_{max}$:

$$\lambda_{max} = \frac{2}{l_0^2}\left(\frac{b+D}{2} - \sqrt{bD}\right), \tag{6.12}$$

$$q_{max} = \frac{1}{l_0}\left(\sqrt{\frac{b}{D}} - 1\right)^{1/2}. \tag{6.13}$$

The value q_{max} determines the distance between the rings

$$d = \frac{2\pi}{q_{max}} = \frac{2\pi l_0}{(\sqrt{b/D} - 1)^{1/2}}. \tag{6.14}$$

It is seen from Eqs. (6.12) and (6.13) that the void DDI ($\lambda > 0$) arises with the formation of the ordered

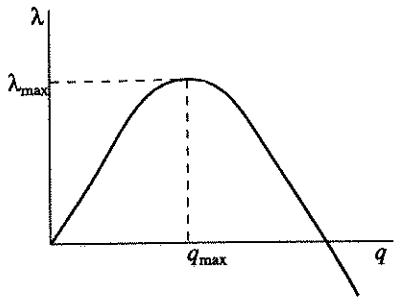

Fig. 28. *Qualitative dependence of the growth rate of the ring periodic structure, according to Eq. (6.11). λ_{max} and $d \equiv 2\pi q_{max}^{-1}$ are the growth rate and the period of the dominant structure, respectively.*

structures (q_{max} is real), provided the threshold condition $b \geq D$ is satisfied, that is,

$$\frac{b}{D} = \frac{\sigma_\perp}{\sigma_\parallel}(N_0 S_0)\frac{|\theta|}{kT} \geq 1. \qquad (6.15)$$

The number density of cylindrical through voids in the film of thickness versus temperature is determined by the equation [19]

$$N_0 = Gh^3 e^{-\frac{\gamma h^2}{kT_0}}, \quad G = G_0 e^{-\frac{E_m}{kT}}, \qquad (6.16)$$

where G_0, γ are the constants, E_m is the activation energy of a vacancy. For T = const, Eqs. (6.14) and (6.16) dictate the following dependence of period d on the film thickness h

$$d \equiv 2\pi l_0 \left[\sqrt{Bh^3 \exp\left(-\frac{\gamma h^2}{kT}\right)} - 1\right]^{-1/2}, \qquad (6.17)$$

where

$$B = \frac{\sigma_\perp}{\sigma_\parallel} S_0 \frac{|\theta|}{kT} G_0 \exp\left(-\frac{E_m}{kT}\right).$$

Thus, for T = const there are two critical values of h, for which $d \to \infty$ (Fig. 32). On the other hand, for h = const there is a certain critical temperature $T = T_{cr}$ (determined from the condition $b = D$) above which the void DDI develops.

6.2. Experimental Investigation of Periodic Void Ring Structure Formation

The formation of the concentric ring void structures was observed under laser vapor deposition of metallic films in Ref. [127]. The experimental setup is shown in Fig. 29. The glass substrate with diameter 80 mm and thickness 2.5 mm was installed in a vacuum camera (10^{-5} torr) and the central part of the substrate was illuminated by CO_2-laser radiation with power 10 W, which was focused to a 1 mm diameter spot. The optical absorption coefficient of glass at the wavelength 10.6 μm is large enough to render the substrate plate optically thick. The substrate plate was heated by laser radiation for 25 min in a vacuum in order to reach a stationary temperature distribution. The gas was then let into the vacuum chamber from a container with carbonyl ($Mo(CO)_6$, $W(CO)_6$, or $Cr(CO)_6$) through the inlet.

The pyrolytic carbonyl dissociation took place near the heated surfaces, which resulted in Mo, W, and Cr film deposition on the substrate. To avoid undesirable effects of laser radiation (melting, surface evaporation, and so on) the deposition was studied on the surface opposite to that absorbing laser radiation. The surface temperature had a bell-shaped distribution with the maximum value $T \approx 500$°C in the center of the laser spot ($r = 0$) and with a halfwidth $r = 5$ mm.

After gas injection a 100 nm thick metallic film was deposited on the surface over a time $t_0 \sim 20 - 30$ s. The film thickness $h(r)$ varied, with its maximum value at $r = 7$ mm. The characteristic radial distribution $h(r)$ for intermediate times is shown in Fig. 27a. At deposition times $t > t_0$, in the vicinity of maximum value $h(r)$, film de-adherence begins to occur in the form of periodic rings centered at $r = 0$.

The investigation of the light transmission of the film revealed in this region the presence of circular, quasiperiodic (with the center at the point $r = 0$) voids (Fig. 31). The radial distribution of a number of these ring voids $\bar{N}(r)$ per unit length is shown in Fig. 27b. This distribution correlates with the distribution $h(r)$ (compare Fig. 27b with Fig. 27a). The characteristic distance between the rings in the region of the maximum distribution $\bar{N}(r)$ is $d = 3 \times 10^{-3}$ cm.

The surface relief of the film, obtained by a profilometer along the coordinate r in the region of maximum $\bar{N}(r)$ also reveals the quasiperiodic concentric voids on the surface with the width $\Delta r \leq 0.4$ μm (Fig. 30). However in the regions $r < r_{max}$ and $r > r_{max}$ ($\max \bar{N}(r) = \bar{N}(r_{max})$) the profilometer did not record such voids, whereas microscopic study of optical transmission and reflection showed a whole set of concentric voids. From this, one may conclude that the voids in these regions have quite a small width, $\Delta r < 0.1$ μm.

6.3. Comparison of Theoretical and Experimental Results

Let us discuss the physical mechanism of the void DDI in more detail. Owing to the initial fluctuating bending deformation, periodic alternations of the stretching and compression arise in the lower and upper

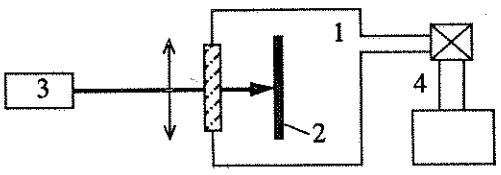

Fig. 29. *Experimental setup. 1 – vacuum chamber, 2 – K-8 glass substrate, 3 – cw CO_2-laser, 4 – inlet and container with carbonyl [127].*